

Global plate boundary evolution and kinematics since the late Paleozoic

Kara J. Matthews^{a*1}, Kayla T. Maloney^a, Sabin Zahirovic^a, Simon E. Williams^a, Maria Seton^a, R. Dietmar Müller^a

^aSchool of Geosciences, University of Sydney, Sydney, NSW 2006, Australia

*Corresponding author: kara.matthews@earth.ox.ac.uk

¹Present address: Department of Earth Sciences, University of Oxford, South Parks Road, Oxford OX1 3AN, UK

Keywords: Alexander Terrane, Paleozoic, Pangea, Panthalassa, plate reconstruction, subduction

Highlights:

- A continuous global plate reconstruction model is presented that spans 410–0 Ma
- The model is digital and open-access
- A new regional model for the Baltica-derived Alexander Terrane is incorporated
- Plate sizes, plate and continent speeds and trench migration patterns are analysed

28 Abstract

29 Many aspects of deep-time Earth System models, including mantle convection, paleoclimatology,
30 paleobiogeography and the deep Earth carbon cycle, require high-resolution plate models that include the
31 evolution of the mosaic of plate boundaries through time. We present the first continuous late Paleozoic to
32 present-day global plate model with evolving plate boundaries, building on and extending two previously
33 published models for the late Paleozoic (410–250 Ma) and Mesozoic-Cenozoic (230–0 Ma). We ensure
34 continuity during the 250–230 Ma transition period between the two models, update the absolute
35 reference frame of the Mesozoic-Cenozoic model and add a new Paleozoic reconstruction for the Baltica-
36 derived Alexander Terrane, now accreted to western North America. This 410–0 Ma open access model
37 provides a framework for deep-time whole Earth modelling and acts as a base for future extensions and
38 refinement.

39 We analyse the model in terms of the number of plates, predicted plate size distribution, plate and
40 continental root mean square (RMS) speeds, plate velocities and trench migration through time. Overall
41 model trends share many similarities to those for recent times, which we use as a first order benchmark
42 against which to compare the model and identify targets for future model refinement. Except for during
43 the period ~260–160 Ma, the number of plates (16–46) and ratio of “large” plates ($\geq 10^{7.5}$ km²) to smaller
44 plates (~2.7–6.6) are fairly similar to present-day values (46 and 6.6, respectively), with lower values
45 occurring during late Paleozoic assembly and growth of Pangea. This temporal pattern may also reflect
46 difficulties in reconstructing small, now subducted oceanic plates further back in time, as well as whether a
47 supercontinent is assembling or breaking up. During the ~260–160 Ma timeframe the model reaches a
48 minima in the number of plates, in contrast to what we would expect during initial Pangea breakup and
49 thus highlighting the need for refinement of the relative model. Continental and plate RMS speeds show an
50 overall increase backwards through time from ~200 to 365 Ma, reaching a peak at 365 Ma of >14 and >16
51 cm/yr, respectively, compared to ~3 and ~5 cm/yr at present-day. The median value of trench motion
52 remains close to, yet above 0 cm/yr for most of the model, with a dominance in positive values reflecting a
53 prevalence of trench retreat over advance. Trench advance speeds are excessive during the period 370–160
54 Ma, reaching more than four times that observed at present-day. Extended periods of trench advance and

55 global continental and plate RMS speeds that far exceed present-day values warrant further investigation.
56 Future work should test whether alternative absolute reference frames or relative motions would mitigate
57 these high speeds, while still being consistent with geologic and geophysical observations, or alternatively
58 focus on identifying potential driving mechanisms to account for such rapid motions.

59 **1 Introduction**

60

61 Progress in plate reconstruction modelling over the past 30 years (e.g. Scotese and McKerrow, 1990;
62 Lithgow-Bertelloni and Richards, 1998; Scotese, 2001; Cocks and Torsvik, 2002; Stampfli and Borel,
63 2002; Torsvik and Cocks, 2004; Torsvik et al., 2014), coupled with technological advances in open
64 source reconstruction software (e.g. GPlates – Boyden et al., 2011), has led to a generation of high
65 spatial and temporal resolution models that describe the continuous evolution of whole plates,
66 including their boundaries (Gurnis et al., 2012; Seton et al., 2012, Shephard et al., 2013; Domeier et al.,
67 2014; Gibbons et al., 2015; Zahirovic et al., 2014; Domeier et al., 2015). This current generation of
68 models is open-access (e.g. rotation and geometry files are freely available), and thus quantifiable,
69 reproducible and adaptable. This enables testability and improvements in a community framework,
70 and makes such models more accessible to complementary fields such as geology, geodynamics,
71 paleobiogeography and paleoclimatology.

72

73 Plate tectonic reconstructions that incorporate evolving global plate boundaries can be integrated in
74 numerical models of mantle convection as a surface boundary condition. Importantly, as they
75 reconstruct subduction histories, that is, they predict where and when slabs entered the mantle, they
76 enable the exploration of whole mantle evolution and the history of surface vertical motions, including
77 dynamic and tectonic topography, over timeframes of hundreds of millions of years. Early
78 investigations (e.g. McNamara and Zhong, 2005; Zhang et al., 2012; Flowers et al., 2012) adopted static
79 reconstructions, with stages that were tens of millions of years long (e.g. Scotese; Lithgow-Bertelloni
80 and Richards, 1998). Now, reconstructions with evolving time-dependent plate boundaries (resolved
81 topologies – Gurnis et al., 2012) that enable the calculation of plate velocities and plate boundary

82 geometries at much shorter intervals, are being used to investigate long-term mantle circulation
83 (Bower et al., 2013; Hassan et al., 2015; Hassan et al., 2016), the degree-structure of the lower mantle
84 (Bull et al., 2014; Zhong and Rudolph, 2015) and surface topographic evolution (Shephard et al., 2014;
85 Flament et al., 2015).

86
87 Reconstructing subduction histories also enables the investigation of deep Earth-atmospheric
88 relationships, such as the deep Earth carbon cycle. Subduction zone volcanism significantly affects the
89 atmospheric carbon budget over geological time via the production of large volumes of CO₂ (Berner et
90 al., 1983; van der Meer et al., 2014), and this addition of CO₂ to the atmosphere can be compounded
91 when subduction zones intersect carbonate platforms leading to metamorphic decarbonation (Lee et
92 al., 2013). It is thus useful to be able to estimate changes in subduction zone length, and associated
93 slab flux approximations, and subduction zone location over time. Existing studies are limited and
94 have focused on the Mesozoic (e.g. Berner et al., 1983; Lee et al., 2013; van der Meer et al., 2014)
95 leaving room for exploration into deeper time. Estimates for changes in ridge length, particularly
96 during major continental breakup phases are also important for studying atmospheric compositional
97 fluctuations over deep time. Volcanism at shallow ridges, such as those that form during continental
98 breakup, can contribute important changes to seawater chemistry, which in turn can affect ocean
99 primary productivity and atmospheric O₂ levels (Gernon et al., 2016).

100
101 A single, global topological model with high spatio-temporal resolution that spans supercontinent
102 assembly and dispersal, even that of the most recent supercontinent Pangea, is currently lacking, yet is
103 essential for addressing ongoing questions about supercontinent cycles, mantle evolution, dynamic
104 topography and the deep Earth carbon cycle over timeframes of hundreds of millions of years.
105 Although reconstructions with resolved topologies exist for the late Paleozoic from 410–250 Ma
106 (Domeier and Torsvik, 2014) and Mesozoic-Cenozoic from 230–0 Ma (Müller et al., 2016) or 200–0 Ma
107 (Seton et al., 2012), different methodologies for connecting plate models will likely result in different
108 velocities during the connection period that can be tens of millions of years long (Zhong and Liu, 2016)
109 making it difficult to directly compare results from individual studies. Furthermore, access to a

temporally continuous model avoids potential plate or numerical modelling artefacts arising from combining models that are not regionally consistent with each other.

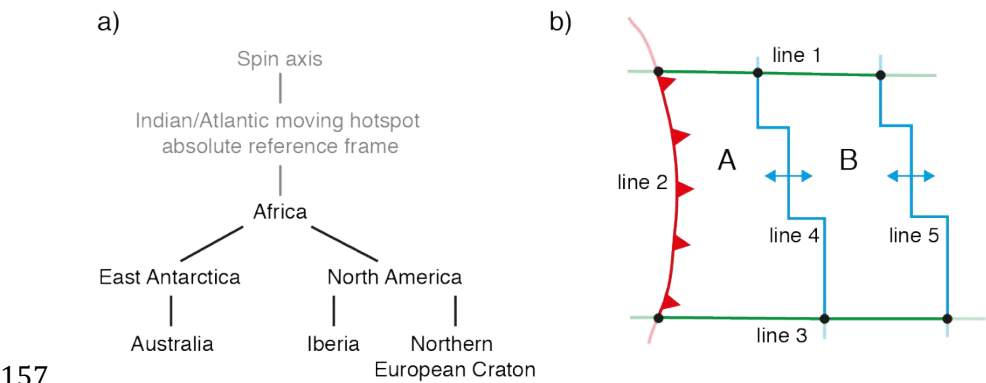
To contribute to studies of long-term surface-mantle-atmospheric evolution incorporating supercontinent assembly and dispersal, we have seamlessly merged two published global plate reconstruction models with resolved topologies (Domeier et al., 2014; Müller et al., 2016), resulting in a continuous self-consistent model that spans 410 Ma to present-day. We have additionally built a late Paleozoic reconstruction for the Baltica-derived Alexander Terrane and implemented a model for the Gravina Basin during the Jurassic, both of which affect the evolution of western North America and subduction history of Panthalassa. The complete model is analysed in terms of the number of plates, predicted plate size distribution, plate and continental root mean square (RMS) speeds, plate velocities and trench migration through time, with the aim of quantifying the model, identifying major trends and isolating potential key targets for future model refinement.

2 Plate model construction

Our late Paleozoic to present-day global plate kinematic model (410–0 Ma) with continuous plate boundaries is primarily constructed from two published plate models. For the period from 410 to 250 Ma we adopt the model of Domeier and Torsvik (2014), and for the period from 230 Ma to present-day we adopt the model of Müller et al. (2016), except with an alternative absolute reference frame from 230 to 70 Ma. Hereafter we refer to these models as DT14 and M16, respectively. Both of these published models are global in spatial extent, based on the reconstruction of rigid plates (i.e. they exclude explicit modelling of deforming regions), and incorporate a dynamic network of continuous plate boundaries with resulting plate polygons.

2.1 Model construction

136 The construction of global plate kinematic models that incorporate a network of continuously
 137 intersecting and evolving plate boundaries is comprehensively described in the reviews of Seton et al.
 138 (2012) and Müller et al. (2016), based on the method described in Gurnis et al. (2012). More
 139 information, particularly relating to the construction and evaluation of an absolute reference frame
 140 and the incorporation of paleomagnetic constraints, can be found in Torsvik et al. (2008a) and
 141 Domeier and Torsvik (2014).
 142
 143 The combined plate model we present is a relative plate motion model that is ultimately tied to Earth's
 144 spin axis via an absolute reference frame. Other than Africa, the motion of any given plate is described
 145 relative to an adjacent plate numerically using a finite Euler rotation. The motion of all plates is tied,
 146 via plate motion chains, to Africa (Figure 1a), which is traditionally considered the base of the plate
 147 'hierarchy' due to its minimal longitudinal motion since Pangea and its position in the core of both
 148 Pangea and Gondwana (e.g. Burke and Torsvik, 2004; Torsvik et al., 2008a; Torsvik et al., 2008b). The
 149 motion of Africa is subsequently linked to the base of the mantle via a True Polar Wander-corrected
 150 absolute reference frame model. An exception to this is the treatment of plates in the
 151 Pacific/Panthalassic realm for times before 83 Ma, due to the lack of a shared seafloor spreading
 152 centre between the Pacific and West Antarctica, which only exists since the Late Cretaceous. For older
 153 times the Pacific/Panthalassa is surrounded by subduction zones and their constituent plates cannot
 154 be linked to a plate hierarchy with Africa at its base. As a result, plates in the Pacific/Panthalassa
 155 require a separate absolute reference frame for times older than 83 Ma, one that is also tied to the spin
 156 axis.



157
 158 **Figure 1**

(a) A subset of the global plate hierarchy for the Cenozoic. For example, the motion of Australia is described relative to East Antarctica, and the motion of East Antarctica is described relative to Africa. Africa is at the base of the hierarchy, and its motion is tied to the absolute reference frame, which at this time is an Indian/Atlantic moving hotspot reference frame (Torsvik et al., 2008). This reference frame is anchored to the spin axis. (b) Schematic illustrating the construction of a resolved topology. Plate A is formed by the intersection of lines 1-4 and Plate B is formed by the intersection of lines 1 and 3-5. Individual plate boundary lines can be used to define multiple plates, yet only the portion of the lines between the plate boundary intersection points (filled black circles) participate in the topology. As the plate boundaries rotate through time the plate will grow or shrink accordingly. The dark segments of the lines are participating in the topologies of plates A and B at this time, while the transparent segments of the lines are not.

Both the input global reconstruction models (DT14 and M16) and the resulting 410–0 Ma model presented here were constructed using the GPlates open-source plate reconstruction software (Boyden et al., 2011; Gurnis et al., 2012). GPlates enables plates and their boundaries to be reconstructed using Euler rotation parameters. The motion of subduction zones is fixed to the motion of the overriding plate, while transform boundaries are assigned the motion of either of their adjacent plates. The motion of mid-ocean ridges is automatically computed from that of both of their adjacent diverging plates; they are reconstructed using ‘half-stage rotations’ (see Seton et al., 2012). Finally, GPlates allows for the construction of resolved topologies, which are continuously-closing plate polygons constructed from the intersection of plate boundary polylines (Gurnis et al., 2012) (Figure 1b). In addition to capturing the evolving configuration of plate boundaries, resolved topologies allow for the sampling of velocities across the entire surface of plates, not just for continents.

2.2 Input global models

Models DT14 (Domeier and Torsvik, 2014) and M16 (Müller et al., 2016) are built from the synthesis of a wide variety of geological and paleogeographical data that enable the identification and dating of

187 collisional, transform, rifting and seafloor spreading events, which further permit the construction of
188 plate boundaries and estimation of plate motions. A key difference between the two models, which is a
189 function of their time frames, is that the plate motions of the younger model M16 are largely
190 underpinned by marine geophysical data (e.g. magnetic anomaly picks, fracture zones, extinct ridges,
191 seamount trails, and absolute seafloor ages from deep-sea drilling). The older, model DT14, covers a
192 timeframe for which all seafloor has been subducted, necessitating increased use of paleomagnetic
193 data to supplement information obtained from continental geology.

194

195 **2.2.1 Paleozoic (410–250 Ma): Domeier and Torsvik (2014)**

196 Domeier and Torsvik (2014) presented a global plate reconstruction model, DT14, for the late
197 Paleozoic (410–250 Ma) that was built from the work of Torsvik et al. (2014). They adopt a
198 paleomagnetic absolute reference frame that has been corrected for true polar wander. Paleomagnetic
199 data also form a major constraint on the motion of individual plates, and as a result the motions of
200 several blocks, such as Tarim and Amuria, are stored as Euler rotations relative to the paleomagnetic
201 reference frame. The motions of plates in Panthalassa (Farallon, Phoenix and Izanagi) are each tied to
202 the Panthalassa triple junction point, which in turn moves relative to the paleomagnetic reference
203 frame. Domeier and Torsvik (2014) implement a simple three-plate spreading scenario that maintains
204 circum-Panthalassic subduction over the model timeframe.

205

206 Several modifications to the late Paleozoic plate motion model DT14 were required to facilitate the
207 merge with model M16. The majority of these modifications were minor technical modifications, and
208 did not result in any major changes to the relative plate motions produced by Domeier and Torsvik
209 (2014), and none resulted in a change to their choice of absolute reference frame. Other modifications
210 to their relative motion model were implemented in the Tethys and western North America, and we
211 retained the pre-rift fit of continents that make up Pangea from Müller et al. (2016). The reason for
212 these modifications was to allow for consistency with the younger, and better-constrained, Mesozoic
213 break-up history, which is built from a number of in-depth regional kinematic studies and seafloor
214 data.

215
216
217
218
219
220
221

222

223
224
225
226
227
228
229
230
231
232
233
234
235
236
237
238
239
240
241

Our updated reconstruction for western North America, which largely focuses on episodes of back-arc basin formation and terrane accretion, is described separately in Section 3 as its timeframe straddles both the Paleozoic and early-mid Mesozoic. Furthermore, parts of the model are new, such as the Paleozoic history of the Alexander Terrane and opening and closure of the Gravina Basin in the Jurassic-Cretaceous, thus warranting a detailed description, and discussion of geological constraints.

2.2.1.1 Model technical modifications

The mid-ocean ridges from model DT14 reconstruct relative to the absolute reference frame in the plate hierarchy and have been assigned individual plate reconstruction IDs and Euler rotations. We recreated all mid-ocean ridges, in their same locations, so that they reconstruct in GPlates with half-stage rotations derived from the finite rotations of the plates flanking the ridge. This allows their motion to automatically respond to future relative plate motion model updates. Another such technical modification was the addition of all blocks to the global plate hierarchy, to result in a purely relative plate motion model. The motions of several blocks in the late Paleozoic model of DT14 are constrained by paleomagnetic data and therefore directly tied to the paleomagnetic reference frame rather than an adjacent plate. For such blocks we recalculated their equivalent rotations relative to an adjacent plate, thereby incorporating them in a relative plate motion hierarchy with Africa at its base (see Section 2.1), yet also retaining their overall absolute motion. These recalculations are all identified in the comments section of the accompanying plate motion model rotation file (Supplementary Material). The conversion to a fully relative plate motion model was chosen to maintain consistency with the model of Müller et al. (2016), and facilitate future testing of alternative absolute reference frames by preserving relative plate motions between plates. However, it should be noted that during such testing the latitudes of these blocks may change, and therefore they will need to be reexamined to ensure integrity with paleomagnetic data. Finally, as we have adopted the continental outlines accompanying model M16, several minor modifications to the shapes of plate boundaries were made to ensure that the boundaries continue to reflect the relative motions of adjacent plates. For instance, minor

242 modifications were made to prevent Domeier and Torsvik's (2014) oceanic plate boundaries cutting
243 through continental lithosphere that had not been modelled in DT14.
244

245 A major technical modification to model DT14 involved the reorientation of the spreading ridge triple
246 junction in Panthalassa, comprising the Farallon-Izanagi, Izanagi-Phoenix and Phoenix-Farallon
247 spreading ridges. The triple junction at 250 Ma in model DT14 is located ~3000 km north-northwest
248 of the triple junction at 230 Ma in model M16, and furthermore, there is more than 50° difference in its
249 orientation (Figure 2). For instance, the Phoenix-Farallon ridge is subducting beneath the
250 southernmost tip of South America at 250 Ma in model DT14, whereas it is subducting beneath central
251 South America at 230 Ma in model M16 (Figure 2). As the motions of plates in the Pacific domain are
252 fully or at least partially constrained by magnetic anomalies and fracture zones for much of the
253 Mesozoic and Cenozoic, our triple junction evolution in the late Paleozoic was built to be consistent
254 with model M16 at 230 Ma. We adopted the absolute position of the triple junction and its orientation
255 from model M16 at 230 Ma, and preserved the model DT14 stage rotations for the Farallon, Izanagi
256 and Phoenix plates from 250 Ma back to 410 Ma by recalculating their finite rotation based on the new
257 triple junction location. Therefore, the relative motions of the Panthalassic plates with respect to each
258 other are from Domeier and Torsvik (2014), however their absolute positions have been changed to
259 be consistent with the younger model timeframe in M16.
260
261
262

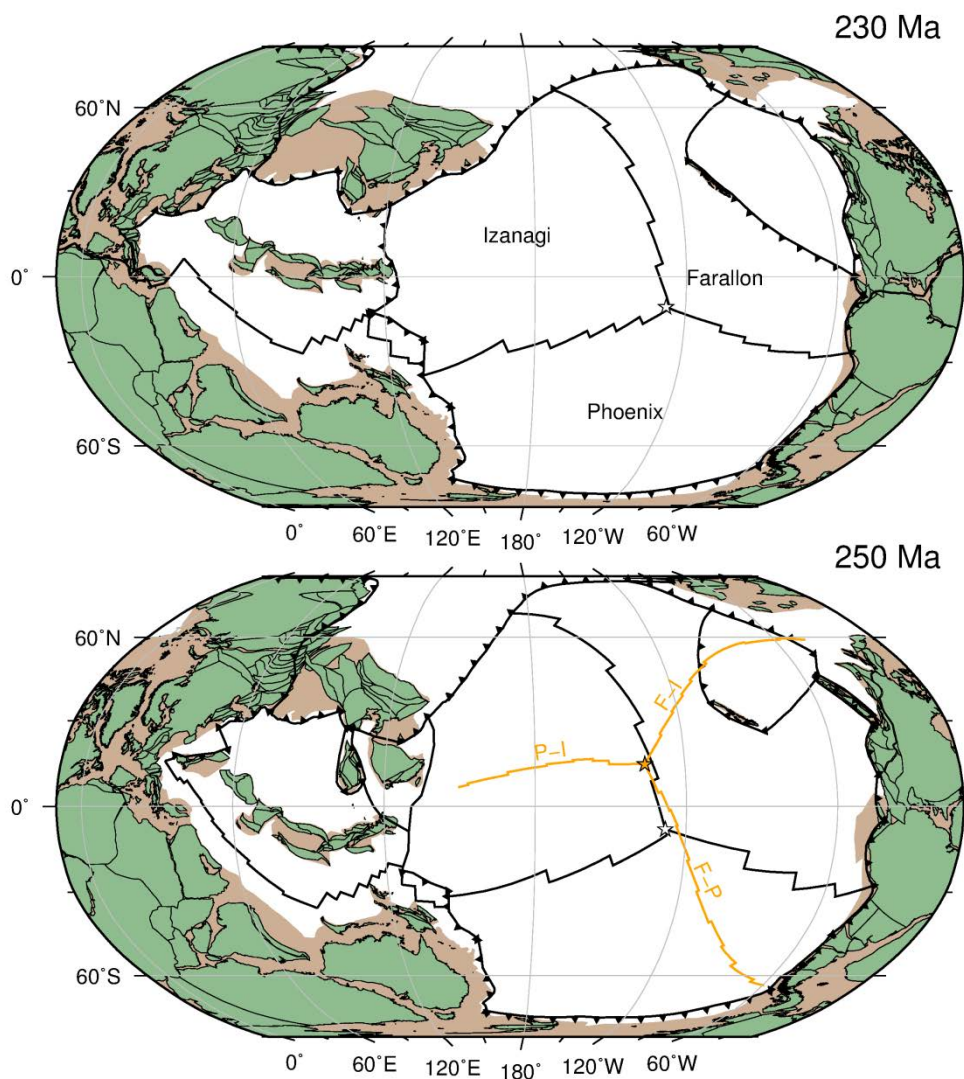


Figure 2

Plate reconstructions at 230 Ma (top) and 250 Ma (bottom) highlighting the location and orientation of the spreading ridge triple junction in Panthalassa (paleo-Pacific) at these times; either end of the 250-230 Ma transition timeframe between input models M16 and DT14. The reconstructions are from the present study, and the triple junction from model DT14 is also shown at 250 Ma (orange lines). The triple junction at 230 Ma has not been modified from model M16, while the triple junction at 250 Ma is in a noticeably different location, and the ridges are at different orientations to model DT14. Although the relative motions for the Phoenix, Izanagi and Farallon plates are retained from DT14 for the late Paleozoic, we adopted the absolute position and orientation of the model M16 triple junction at 230 Ma and recalculated the finite poles of rotation accordingly. F-I, Farallon-Izanagi spreading; F-P, Farallon-Phoenix spreading; P-I, Phoenix-Izanagi spreading. Stars denote the location of the triple junction point.

277 Our modifications to the late Paleozoic Farallon-Izanagi-Phoenix triple junction result in altered
278 relative motions at the Panthalassic rim. We have updated the plate boundaries, where necessary, to
279 be consistent with the new relative motion history. Convergence remains dominant throughout the
280 late Paleozoic around much of its margin. However, our changes to the orientation of the Izanagi-
281 Phoenix spreading ridge have resulted in longer histories of transform or divergent motion to the
282 north and northwest of Australia and New Guinea, in the junction region between Panthalassa and the
283 Tethys, where Domeier and Torsvik (2014) modelled almost continuous subduction (see
284 Supplementary Animation S1 for a comparison of our current model with that of Domeier and Torsvik,
285 2014). We have also updated the 250 Ma Euler rotation for the Phoenix Plate, and the motion of the
286 Gympie-Brook Street terrane to the east of Australia between 270 and 250 Ma, to preserve
287 convergence along eastern Gondwana at a time when evidence of subduction is clearly identified in the
288 geologic record (Domeier and Torsvik, 2014).

289

290 **2.2.1.2 Tethys model updates**

291 Modifications to model DT14 in the Tethys region were required to facilitate the merge with model
292 M16. These include adjustments to the motions of the Cimmerian terranes that rifted from northern
293 Gondwana at 275 Ma, as well as South China and Indochina (Annamia) that started rifting from
294 Gondwana prior to the beginning of the model at 410 Ma.

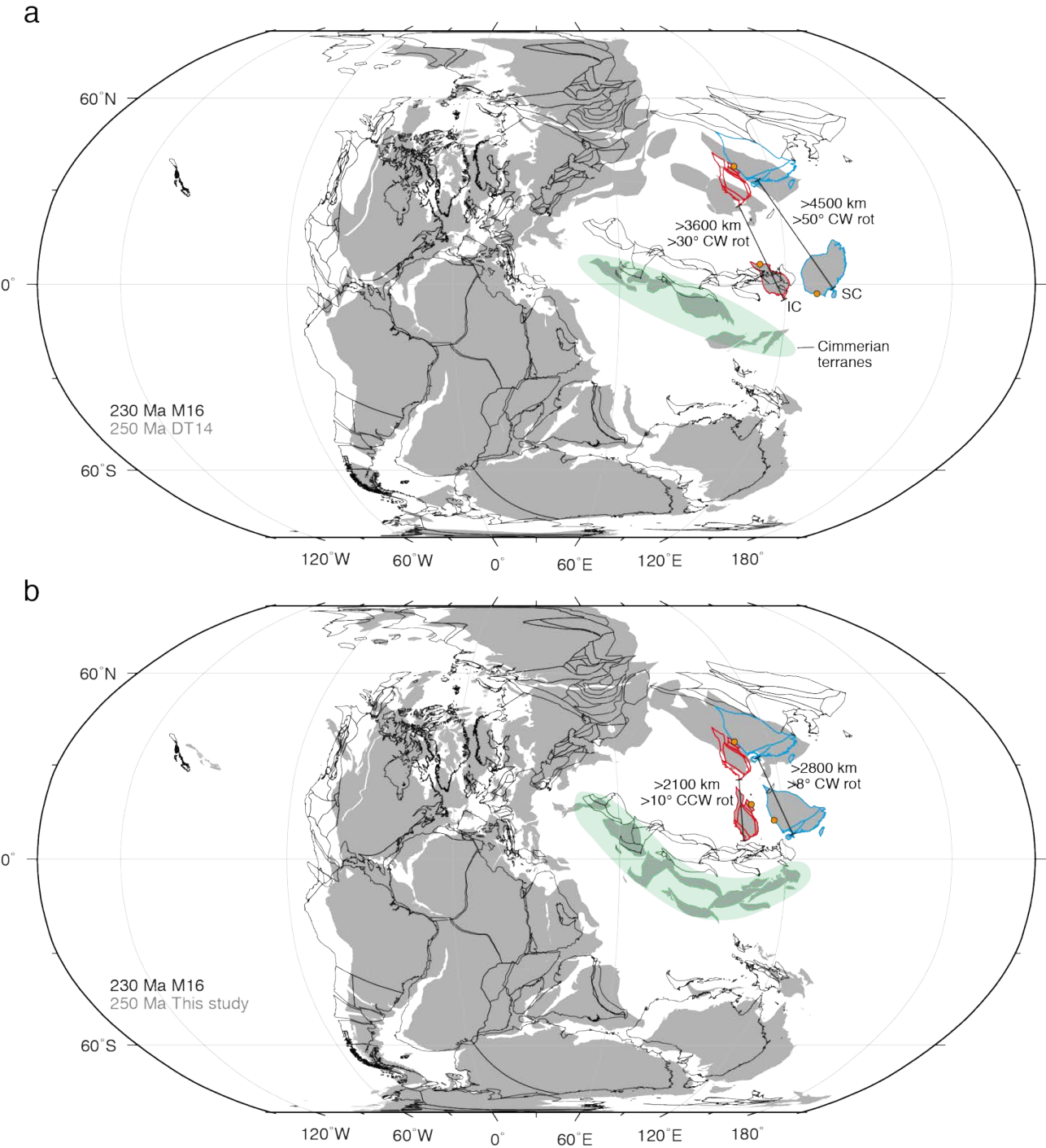
295

296 **> South China and Indochina**

297 For times older than 360 Ma we have made minor adjustments to the absolute positions of Indochina
298 and South China. Although the style of relative motion between the two blocks, such as divergent or
299 convergent, remains unchanged, to avoid overlap caused by adopting different continental block
300 geometries we adjusted their initial 410 Ma positions along the Gondwana margin by less than
301 400 km. From 360 to 260 Ma the motion of South China is described by the rotations from DT14.
302 During this time the Indochina-South China relative motions are also the same as in model DT14,
303 although with higher convergence rates from 270 to 260 Ma.

304

305 After 260 Ma the models for Indochina and South China diverge from that implemented in model
306 DT14. Our modifications were required to accommodate the collision of Indochina and South China at
307 245 Ma, indicated by a cessation of subduction zone magmatism (Liu et al., 2012), and to allow for
308 consistency with the post-250 Ma evolution of blocks in and bordering the Tethys. At the conclusion of
309 model DT14 at 250 Ma, Indochina and South China are separated by ~500 km with the western
310 margin of South China parallel to the eastern margin of Indochina (present-day orientation) (Figure 3).
311 However, as the northern margin of Indochina collides with the southwestern margin of South China
312 at 245 Ma, we modified their motion after 260 Ma to prevent unrealistically fast rotation of Indochina
313 between 250 and 245 Ma.
314



316

317 **Figure 3**

318 (a) Continental reconstructions from model DT14 at 250 Ma (grey) and model M16 at 230 Ma (black outlines)
319 showing the motion required by the continents over the 20 Myr model transition period (250-230 Ma) if no
320 additional rotations are added. While Pangea only needs to migrate <10° westward from 250-230 Ma, the
321 motion of blocks in the Tethyan realm is more complex. For instance, South China (SC, blue outlines) is required
322 to travel >4500 km and rotate >50° clockwise (CW) in order to transition from its 250 to 230 Ma position, and
323 Indochina (IC, red outlines) is required to travel > 3600 km and rotate >30° clockwise. (b) Continental

reconstructions from the present study at 250 Ma (grey) and model M16 at 230 Ma highlighting updates to model DT14 at 250 Ma. For instance, the new trend of the Cimmerian terranes (green) reflects our revision of their pre-rift positions along the Gondwana margin. Additionally, South China and Indochina have been modified to slow down their northward migration (>2800 and >2100 km, respectively) and minimise their rotation ($>8^\circ$ clockwise and $>10^\circ$ counterclockwise, respectively). The filled orange circles on the margins of South China and Indochina at 250 Ma must overlap at 230 Ma due to their collision at 245 Ma.

We initiate northward motion of Indochina and South China towards North China at 260 Ma, rather than at 250 Ma after model DT14 ends, in order to prevent potentially unreasonably fast motion of South China during its journey towards North China. We model collision of North China and South China at 230 Ma, 20 Myr beyond the DT14 model timeframe. Our implementation of collision at 230 Ma coincides with an ultra-high pressure coesite-eclogite metamorphic event described by Wu and Zheng (2013). By adopting the position of South China at 250 Ma from model DT14, South China would have to travel more than 4500 km and rotate by more than 50° in 20 Myr to collide with North China at 230 Ma (Figure 3). This may be unrealistically high considering that South China is such a large continental block, and 20 cm/yr is considered as a tectonic speed limit usually only exceeded by small continental blocks on large oceanic plates in the post-Pangea timeframe (Zahirovic et al., 2015). Based on our modification South China travels ~ 2800 km and rotates by about 8° during this 20 Myr timeframe (Figure 3). This adjustment to the position of South China is also important as the collision may have occurred even earlier (Wu and Zheng, 2013), which would result in an even shorter period of time to travel more than several thousand kilometres.

Finally, our new post 260 Ma motions for Indochina and South China also prevent overlap or close interaction with the Cimmerian terranes during their migration towards southern Eurasia. Our modifications to the motion of South China between 260 and 250 Ma requires the opening of a back-arc basin to the east of South China along the western margin of Panthalassa to prevent rapid trench advance. This short-lived basin is model dependent and all crust created during this time is later subducted. Despite our modifications to Indochina and South China motions their plate boundaries

352 remain largely unchanged during this timeframe reflecting similar relative motions with neighbouring
353 plates (Supplementary Animation S1).

354

355 **> North China and Amuria**

356 The motion of North China is described relative to the absolute reference frame in model DT14. In
357 order to include North China in a plate hierarchy we have calculated equivalent rotations for North
358 China relative to adjacent plates with which it shares a divergent or transform boundary, where
359 possible. Despite minor adjustments that were made during the process of integrating North China in a
360 plate hierarchy, North China remains within 5–10° latitude of its DT14 position, thereby preserving
361 integrity with paleomagnetic constraints.

362

363 In addition to our North China and South China collision model, described above, we implement
364 collision between Amuria and North China, along the northern margin of North China. This event was
365 associated with closure of the Paleoasian Ocean. This latter event is not well constrained, possibly
366 occurring in the late Permian–Triassic, so we model collision at 250 Ma, as tentatively suggested by
367 Domeier and Torsvik (2014).

368

369 **> Cimmerian terranes and other western Tethyan blocks rifted from Gondwana**

370 We adopted the pre-rift positions of Lut, Iran and Afghanistan along northern Gondwana from Müller
371 et al. (2016). This results in the blocks being 500–1000 km west of their positions in model DT14. We
372 also modified the pre-rift positions of Lhasa, Qiangtang, Sibumasu and the Malay Peninsula from
373 model DT14 to be around 400 km further west. We additionally separated the Lhasa and Qiangtang
374 blocks, placing Lhasa closer to the northwest Australian margin and leaving Qiangtang near the Indian
375 margin of Gondwana. This was to satisfy detrital zircon constraints that reveal an Australian affinity
376 for Lhasa, in contrast to a ‘High Himalaya’ affinity for Qiangtang (Zhu et al., 2011). These modified
377 placements avoid overlap of Sibumasu with Lhasa, and the Malay Peninsula with the Bird’s Head
378 blocks west of New Guinea, yet remain consistent with geological observations. See Figure 3 for the
379 alternative configurations of the so-called Cimmerian terranes at 250 Ma.

380

381 Our model for the western Tethys blocks, such as the Pontides, including their pre-rift placement along
382 Gondwana is taken from previous works (Schettino and Turco, 2011; Hosseinpour et al., 2016).
383 Although we retain the Domeier and Torsvik (2014) relative motion model for Iberia, its absolute
384 position along Gondwana and therefore relative to Armorica, is based on Barnett-Moore et al. (in
385 press).

386

387 2.2.2 Late Triassic to present-day (230–0 Ma): Müller et al. (2016)

388 The recent global plate motion model M16, is an update of the Seton et al. (2012) plate model. It
389 incorporates new regional reconstructions for the Arctic, Eastern and Western Tethys, Southwest
390 Pacific, Southeast Asia, Pacific, North and South Atlantic, and Caribbean. Model M16 is a purely relative
391 plate motion model with Africa at the base of the plate hierarchy. No other plate, except for the Pacific
392 at certain times in the Mesozoic, is tied directly to the absolute reference frame. Africa is tied to the
393 spin axis via a combination of absolute frames. During the period from 0 to 70 Ma, Müller et al. (2016)
394 adopt a global moving hotspot reference frame (Torsvik et al., 2008), and for the period from 100 to
395 230 Ma they adopt a True Polar Wander (TPW)-corrected paleomagnetic reference frame (Steinberger
396 and Torsvik, 2008) to which a 10° longitudinal shift is applied to produce a smooth transition between
397 the two reference frames. No finite poles of rotation are incorporated in the model during this 30 Myr
398 transition period between reference frames (70–100 Ma), however it should be noted that during this
399 interval GPlates interpolates between the rotation poles at 70 and 100 Ma. Plates in the Pacific Ocean
400 basin are tied to a fixed Pacific hotspot reference frame for times older than 83 Ma (Wessel and
401 Kroenke, 2008; Seton et al., 2012). This is necessary as prior to the establishment of seafloor
402 spreading between the Pacific plate and West Antarctica at ~83 Ma the Pacific Ocean basin was
403 entirely surrounded by subduction zones and the motions of its plates cannot be directly tied to Africa
404 via a plate motion chain.

405

406 The main adjustments made to model M16 (i.e. for times younger than 230 Ma), in order to produce a
407 continuous late Paleozoic to present-day kinematic model, are related to the motion of the Wrangellia

408 Superterrane and its collision with western North America. We updated the existing model of closure
409 of the Cache Creek Ocean between the Alexander and Wrangellia terranes (belonging to the Wrangellia
410 Superterrane) and western North America (Shephard et al., 2013) and introduced a model for opening
411 and closure of the Gravina Basin behind the Wrangellia Superterrane in the mid Jurassic to Early
412 Cretaceous. Our new model for the Alexander and Wrangellia terranes, which begins with the rifting of
413 the Alexander Terrane from northern Baltica in the Devonian (400 Ma), is described in detail in
414 Section 3.

415

416 **2.2.2.1 Reference frame update**

417 For the period from 100 to 230 Ma we implement an alternative absolute reference frame to that used
418 by Müller et al. (2016). We adopt the more recent TPW-corrected paleomagnetic reference frame of
419 Torsvik et al. (2012), to which we apply a longitudinal shift. Specifically, we apply a 10° westward
420 longitudinal shift to the raw paleomagnetic reference frame before reapplying Torsvik et al.'s (2012)
421 true polar wander correction. Longitudinal corrections rectify mismatches between surface geology
422 and correlated mantle structures such as subducted slabs and plumes (van der Meer, 2010), and are
423 permissible as longitude cannot be constrained by paleomagnetic data. Our choice of 10° is after
424 Müller et al. (2016) and is consistent with recent studies (van der Meer, 2010; Butterworth et al.,
425 2014; Williams et al., 2015). It is important to note that true polar wander corrections are dependent
426 on the original plate motion model used to derive them, however, we have adopted the published
427 correction of Torsvik et al. (2012) as it was beyond the scope of this study to generate a workflow for
428 calculating true polar wander corrections. We therefore emphasise that future work should focus on
429 updating the true polar wander correction, and this should ideally be repeated whenever the relative
430 plate motion model is updated.

431

432 The choice of absolute reference frame is strongly governed by the purpose of the plate reconstruction
433 model (Torsvik et al., 2012; Williams et al., 2015). A key aim of our study was to produce a continuous
434 plate kinematic model that can be used in global models of mantle convection. We therefore sought to
435 minimize the occurrence of geodynamically unreasonable behaviour, particularly related to

subduction histories. This motivated us to include 20–30 Myr transition periods between references frames, from 70 to 100 Ma and from 230 to 250 Ma, to avoid excessive net rotation and unreasonably rapid or erratic trench migration. To make the plate model more versatile and easily adaptable for other studies, the longitudinal shift and true polar wander corrections, at all times, are stored separately in the plate model rotation file. This allows for simpler testing of alternative references frames, longitudinal shifts and importantly the implementation of up-to-date true polar wander corrections.

443

2.2.3 250–230 Ma model transition period

The Early and Middle Triassic, from 250 to 230 Ma, form the transition period between the two input plate reconstruction models, DT14 and M16. During this 20 Myr timeframe there is incipient rifting within Pangea between North America and Europe in the north, and Africa and South America in the south. These are the early stages of separation of Laurasia and Gondwana. The two major oceanic realms at this time include Panthalassa and the Tethys. In Panthalassa the Phoenix, Farallon and Izanagi plates continue to subduct beneath the Panthalassic rim. Along western North America the Slide Mountain Ocean is in the final stages of closure, while the Alexander and Wrangellia terranes continue to migrate into Panthalassa (see Section 3). In the Tethyan realm the continental fragments derived from northern Gondwana, Cimmerian terranes, continue their northward journey towards the Asian blocks, including North China, South China and Indochina. To the north of the Cimmerian terranes the Paleotethys Ocean is closing, while to the south the Mesotethys Ocean is opening.

456

Generally during this timeframe we allow plates to transition from their 250 Ma position to their 230 Ma, or younger, position as defined in the M16 model, without modifying their motions at intervening times. During this timeframe we also allow for the transition between the absolute reference frame adopted in model DT14 and the updated M16 model reference frame implemented after 230 Ma.

461

Several continental blocks, such as along the Tethyan margin of Australia (e.g., Argoland), Papua New Guinea (e.g., the Sula Spur) and southern Europe (e.g., the Scythian and Karakum blocks) appear in our

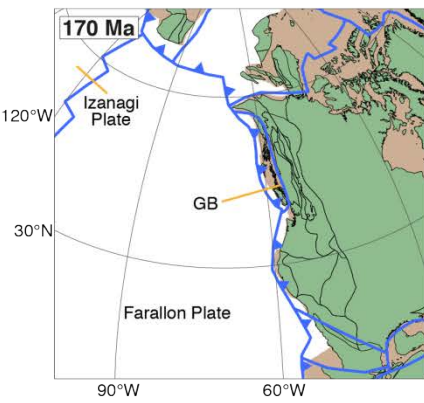
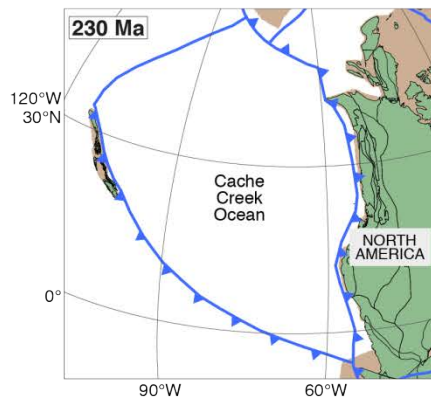
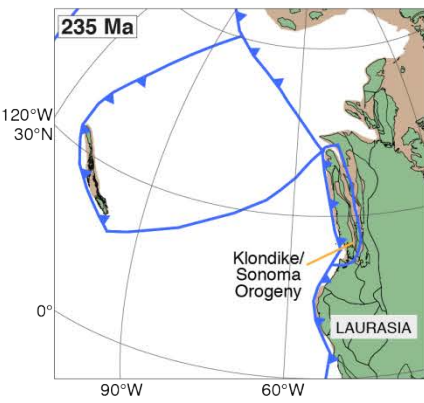
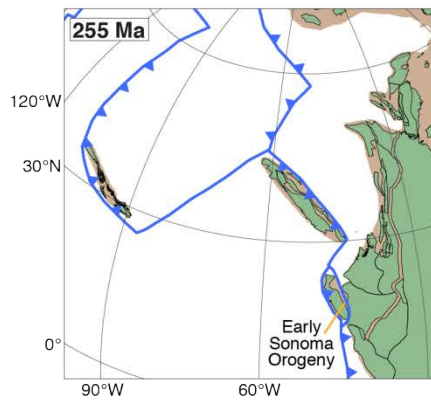
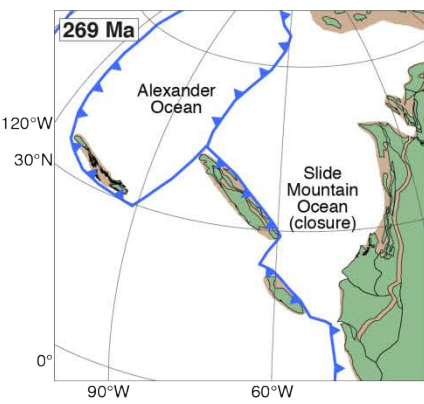
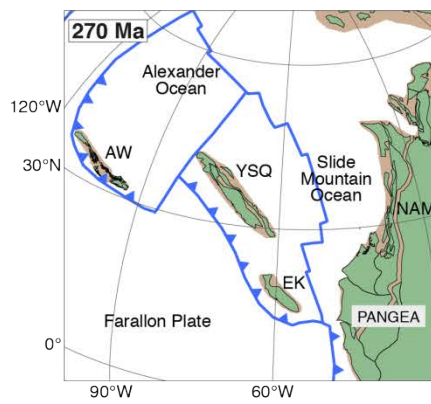
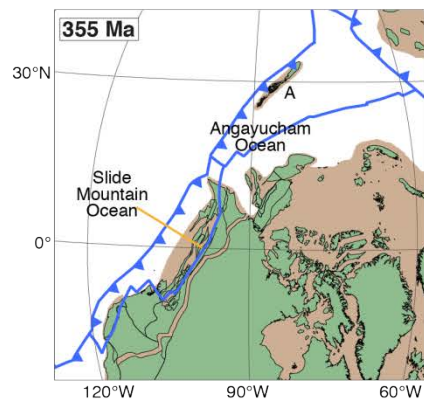
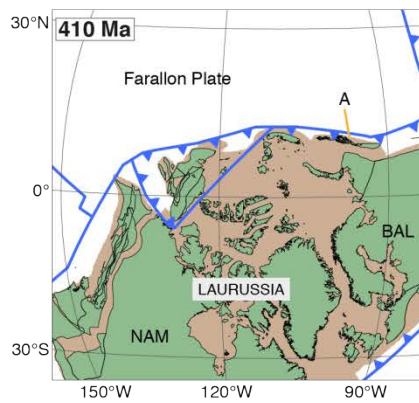
464 model at 250 Ma. This appearance time is not intended to reflect their formation at 250 Ma, rather it is
465 a consequence of the model merge process. Müller et al. (2016) explicitly modelled the histories of
466 these blocks that have ages of at least 250 Ma, however they were not modelled separately by Domeier
467 and Torsvik (2014). It was beyond the scope of this investigation to build new late Paleozoic regional
468 reconstructions for all the continental blocks that were considered in model M16, and therefore we
469 introduce them at 250 Ma.

470 **3 Western North America model updates**

471

472 We have updated the model of Domeier and Torsvik (2014) for the late Paleozoic tectonic evolution of
473 western North America to largely follow the reconstructions of Shephard et al. (2013) and Colpron
474 and Nelson (2009). Shephard et al. (2013) presented a review of the Permian to Cretaceous tectonic
475 evolution of the Arctic and cordilleran western North America based on a detailed synthesis of
476 geological and geophysical data. They also produced a quantitative regional plate kinematic model
477 with evolving topologies from 200 Ma, embedded within a global plate model (Seton et al., 2012).
478 Colpron and Nelson (2009) presented a regional reconstruction of the evolution of western North
479 America from the Early Devonian (~395 Ma) to Early Triassic (~250 Ma). Their work focused on the
480 rifting of the Alexander Terrane from northern Baltica in the Early Devonian, and its motion along
481 northern Laurentia, into Panthalassa. We have also updated the Müller et al. (2016) timing for the
482 amalgamation of the Wrangellia and Alexander terranes with western North America, and added a
483 model for the subsequent opening and closure of the Gravina Basin that is largely based on the work of
484 Kapp and Gehrels (1998). Kapp and Gehrels (1998) tested five alternative Gravina Basin models by
485 analysing detrital zircon provenance and age patterns. Key stages in the model are shown in Figure 4,
486 and in a global context in Figure 5 (also see Supplementary Animation S2).

487



489 **Figure 4**

490 Key stages in our reconstruction of the Alexander Terrane and revised model for the evolution of western North
491 America. The Alexander Terrane is positioned along the Baltican margin at the beginning of the model (410 Ma)
492 and begins to rift away at 400 Ma. Migration of the Alexander Terrane towards Panthalassa is associated with
493 back-arc basin opening along the Laurussian margin. By 355 Ma rifting has propagated southward and the Slide
494 Mountain Ocean starts opening behind the Yukon-Tanana, Stikinia, Quesnellia and Eastern Klamath terranes.
495 The Slide Mountain Ocean and its northward extension behind the Alexander and Wrangellia terranes continue
496 to widen until 270 Ma. At 270 Ma there is a subduction polarity reversal that initiates closure of the Slide
497 Mountain Ocean, however further north the Alexander and Wrangellia terranes continue to migrate into the
498 interior of Panthalassa. During closure of the Slide Mountain Ocean the Yukon-Tanana, Stikinia, Quesnellia and
499 Eastern Klamath terranes move with the Farallon Plate. Two key stages in the diachronous closure of the Slide
500 Mountain Ocean are shown at 255 and 235 Ma, and are associated with the Sonoma and Klondike orogenies. By
501 230 Ma the Slide Mountain Ocean has completely closed and there is a subduction polarity reversal across the
502 Alexander and Wrangellia terranes. Alexander and Wrangellia migrate towards North America. The intervening
503 ocean (Cache Creek) is contemporaneously subducted beneath the Alexander and Wrangellia terranes in the
504 west and North America in the east. Following collision of the Alexander and Wrangellia terranes with western
505 North America at ~180 Ma we model sinistral transtensional opening of the Gravina Basin from 170-155 Ma, and
506 sinistral transpressional closure from 155-140 Ma. See text for a more detailed description of the reconstruction.
507 A, Alexander Terrane; AW, Alexander and Wrangellia terranes; BAL, Baltica; EK, Eastern Klamath; GB, Gravina
508 Basin; NAM, North America; YSQ, Yukon-Tanana, Stikinia and Quesnellia terranes.

510 **3.1 History of back-arc basins**

511 The late Paleozoic to Cretaceous history of western North America was dominated by episodes of
512 back-arc basin opening and closure. The most prominent of these events related to the formation of
513 the widely studied Slide Mountain Ocean that began opening in the Late Devonian behind a collage of
514 western Laurentia-derived (Colpron and Nelson, 2009; Shephard et al., 2013) and potentially Baltica-
515 derived continental fragments (Colpron and Nelson, 2009). The Slide Mountain Ocean back-arc rift
516 system was the southern extension of a back-arc rift system that initiated in the Early Devonian along
517 northern Laurentia (Miller et al., 2011; Beranek et al., 2013), that we model as extending eastward

518 along northern Baltica. This northern Laurentia rift system also led to formation of the comparatively
519 lesser-studied Angayucham Ocean along the margin of Arctic Alaska (e.g. Miller et al., 2011; Beranek et
520 al., 2013). Closure of the Slide Mountain Ocean in the Triassic (e.g. Dickinson, 2006; Nelson et al., 2006;
521 Colpron and Nelson, 2009; Beranek and Mortensen, 2011) resulted in growth of the western margin of
522 Laurentia from crustal and arc accretion events. Remnants of the Angayucham Ocean are preserved in
523 Alaska (Moore et al., 1994).

524

525 Our model for the opening of the Slide Mountain Ocean is based on the work of Colpron and Nelson
526 (2009), and our model for its closure is updated from Shephard et al. (2013). We have not built a
527 specific model for the closure of the Angayucham Ocean, however, the seafloor outboard of Arctic
528 Alaska, that would have formed part of this basin, is subducted during the Early Cretaceous at the
529 Koyukuk and Nutesyn arcs of Shephard et al. (2013).

530

531 Although not strictly modelled as a back-arc basin, we also consider the evolution of the Cache Creek
532 Ocean in our updated tectonic evolution of western North America. The Cache Creek Ocean basin
533 existed adjacent to western North America during the Triassic to Jurassic in the model of Shephard et
534 al. (2013), yet there exists a range of models for its origin and evolution (see also Mihalynuk et al.,
535 1994; Mihalynuk et al., 2006; Colpron et al., 2015). Its closure followed that of the Slide Mountain
536 Ocean.

537

538 **3.2 Reconstruction model**

539 The Alexander Terrane forms part of the western North American cordillera. Its Mesozoic tectonic
540 evolution is incorporated in model M16, yet as its Paleozoic evolution is not incorporated in model
541 DT14 we have built a reconstruction for its kinematic history that extends back to 400 Ma (Figure 4).

542

543 The Alexander Terrane is widely believed to be exotic to western North America (e.g. Gehrels and
544 Saleeby, 1987; Gehrels et al., 1996). For example, the Alexander Terrane has different detrital zircon
545 signatures to the adjacent North American-derived Yukon-Tanana Terrane (Tochilin et al., 2014), and

546 there is no available North America source for 1.48–1.53 Ga aged detrital zircons (Bazard et al., 1995).
547 Its origin is however uncertain, and eastern Australia (Gehrels and Saleeby, 1987; Gehrels et al., 1996),
548 northern Baltica (Bazard et al., 1995; Gehrels et al., 1996; Butler et al., 1997; Colpron and Nelson,
549 2009; Miller et al., 2011; Beranek et al., 2013; Tochilin et al., 2014), southwestern Baltica (Wright and
550 Wyld, 2006; Grove et al., 2008), Siberia (Blodgett et al., 2010) and near the northern margin of
551 Laurentia-Baltica (Soja and Antoshkina, 1997) have all been proposed based primarily on faunal
552 affinities, paleomagnetic data and detrital zircon provenance studies. Following the model of Colpron
553 and Nelson (2009), we place the Alexander Terrane at the northern most margin of Baltica, close to
554 Laurentia, in the Early Devonian (Figure 4). A northern Baltica origin is consistent with many previous
555 studies, is the most kinematically plausible scenario and is the simplest history to implement in the
556 DT14 model. An eastern Australian origin is unlikely, as such a reconstruction would require the
557 terrane to traverse southern Panthalassa, which at this time is modelled with a major long-lived
558 spreading system active between the Phoenix and Farallon plates. A southwestern Baltica origin
559 would require a >10 000 km passage of the Alexander Terrane through the Rheic Ocean, which
560 undergoes both convergent and divergent phases during the Devonian and Carboniferous (Domeier
561 and Torsvik, 2014), and northward along the entire western margin of Laurentia. Finally, Siberia is
562 located ~10 000 km from western Laurentia in the Devonian (Domeier and Torsvik, 2014) requiring
563 high (>20 cm/yr) absolute plate velocities to bring the terrane to the western Laurentian margin by
564 the Carboniferous. Although plate velocities of this order of magnitude are dynamically plausible,
565 particularly for oceanic plates with minor continental areas (Zahirovic et al., 2015), a Baltica origin is
566 preferred. The Alexander Terrane's Early Devonian Karheen Formation contains detrital zircon
567 populations of an age range preserved in rocks from the Scandinavian margin of Baltica, and its
568 placement along the northern Baltic margin also matches paleomagnetic latitudinal constraints
569 derived from the same formation (Butler et al., 1997).

570

571 We model the Alexander Terrane as part of northernmost Baltica in the Early Devonian. Episodic arc
572 magmatism is recorded in the southern Alexander Terrane from as early as the Ediacaran, with arc
573 building stages interrupted by orogenic events, such as the pre-Early Ordovician Wales orogeny and

574 the latest Silurian/earliest Devonian Klakas orogeny (Colpron and Nelson, 2011). Arc activity re-
575 established in the Devonian following the Klakas orogeny as recorded in hypabyssal igneous rocks and
576 volcanic strata (Gehrels et al., 1983; Colpron and Nelson, 2009). We do not model the Klakas orogeny
577 and consider that it occurred prior to the beginning of the reconstruction. The Klakas orogeny may
578 have involved the shedding of debris containing Archean and Proterozoic zircons from Baltica to the
579 Karheen Formation (Butler et al., 1997). We model the rifting of the Alexander Terrane from Baltica at
580 400 Ma (Early Devonian) due to back-arc spreading. Continued trench retreat involves the migration
581 of the Alexander Terrane along northern Laurentia towards Panthalassa. Shortly following
582 detachment and migration of the Alexander Terrane away from Baltica the intraoceanic Magnitogorsk
583 Arc accretes to this region of Baltica, its Uralian margin, in the Late Devonian (e.g. Brown et al., 2006).
584 The modelling of back-arc spreading and terrane detachment so close in time to a major and well-
585 studied arc accretion event at the same margin warrants further investigation. Deciphering the early
586 history of the Alexander Terrane during its separation from Baltica, particularly in the context of well-
587 studied regional tectonic events, is clearly an important and ongoing problem.

588

589 Rifting along northern Laurentia, associated with Alexander Terrane detachment, led to formation of
590 the Angayucham Ocean basin along Arctic Alaska (Beranek et al., 2013) (Figure 4). In published
591 tectonic reconstructions the Angayucham Ocean is consistently labelled close to the Arctic Alaska
592 section of the Laurentian margin (Colpron and Nelson, 2009; Beranek et al., 2013), yet back-arc basin
593 spreading behind the Alexander Terrane was extensive, resulting in an ocean that was more than
594 several thousand kilometres in width; wider than the Slide Mountain Ocean to the south (Colpron and
595 Nelson, 2009). Therefore, to avoid confusion we refer to this major ocean basin behind the Alexander
596 Terrane as the Alexander Ocean (Figure 4). We do not create a specific regional model for the history
597 of the Angayucham Ocean.

598

599 By 365 Ma the Alexander Terrane has migrated westward for 35 Myr and is aligned with the western
600 margin of Laurentia. At 355 Ma we model southward propagation of the back-arc spreading centre
601 behind the Alexander Terrane to initiate back-arc rifting and detachment of the Yukon-Tanana and

602 Eastern Klamath terranes from the western margin of Laurentia (Figure 4). The Alexander Terrane
603 continues to migrate into the interior of Panthalassa. For simplicity, we model the amalgamation of the
604 arc-related Wrangellia Terrane, which has Panthalassic affinity (Colpron and Nelson, 2011), with the
605 Alexander Terrane at 340 Ma, in accordance with evidence of pre-mid Pennsylvanian juxtaposition of
606 the terranes (Gardner et al., 1988). More detailed regional history of the evolution of the Wrangellia
607 Superterrane is beyond the scope of this study.

608

609 Back-arc spreading behind the Yukon-Tanana, Stikinia, Quesnellia and Eastern Klamath terranes
610 results in the Carboniferous opening of the Slide Mountain Ocean, which is continuous with the
611 Angayucham Ocean, and subsequently Alexander Ocean in the north (Figure 4). The Stikinia and
612 Quesnellia terranes both intrude and were deposited on the Yukon-Tanana Terrane (Mihalynuk et al.,
613 1994; Nelson and Friedman, 2006). After Shephard et al. (2013) and Colpron and Nelson (2009), the
614 late Paleozoic motion of the Eastern Klamath Terrane of present-day northern California is linked to
615 that of the Yukon-Tanana, Stikinia and Quesnellia terranes, to form the southwestern margin of the
616 Slide Mountain Ocean. Its earlier Paleozoic origin is less certain, however, and unlike the Yukon-
617 Tanana Terrane it may have been exotic to western North America and shared part of its history with
618 the Alexander Terrane (e.g. Grove et al., 2008; Miller et al., 2011). Nelson and Colpron (2009) present
619 a Devonian model for Eastern Klamath during which it migrates along the northern and western
620 margin of Laurentia via transform motion, however, for simplicity we only model its motion after the
621 Carboniferous (from 355 Ma), at which time it was located south of the Yukon-Tanana Terrane.

622

623 The Alexander-Slide Mountain Ocean opens wider and faster in the north behind the Alexander and
624 Yukon-Tanana terranes, compared to farther south behind Eastern Klamath (Nelson and Colpron,
625 2009). Opening of this ocean involves consumption of the Farallon Plate. By the mid Permian, when
626 the Slide Mountain Ocean is at its widest, the Yukon-Tanana, Stikinia and Quesnellia terranes are
627 separated from North America by 2000–3000 km.

628

629 Our model predicts a major reorganisation of spreading in the Slide Mountain Ocean at 270 Ma, at
630 which time there is a subduction polarity reversal and the ocean begins to subduct beneath the Yukon-
631 Tanana, Stikinia, Quesnellia and Eastern Klamath terranes (Figure 4). Our imposed timing of initiation
632 of subduction of the Slide Mountain Ocean is midway between the timings proposed by Domeier and
633 Torsvik (2014) and Shephard et al. (2013) of 280 and 260 Ma, respectively, yet is still consistent with
634 geological observations (Mortensen, 1992; Nokleberg et al., 2000; Nelson et al., 2006; Piercey et al.,
635 2006; Nelson and Colpron, 2011; Saleeby, 2011). Domeier and Torsvik (2014) implement double-
636 dipping subduction during closure of the Slide Mountain Ocean, such that the Slide Mountain Ocean
637 and the Farallon Plate are subducting contemporaneously beneath the Yukon-Tanana, Stikinia and
638 Quesnellia terranes. For consistency with the tectonically simpler model of Shephard et al. (2013) we
639 implement a polarity reversal from northeast to southwest-dipping subduction to initiate closure of
640 the Slide Mountain Ocean, and remove the dual-dipping subduction implemented in model DT14. As a
641 result of the subduction polarity reversal the Yukon-Tanana, Stikinia, Quesnellia and Eastern Klamath
642 terranes move with, and essentially form part of the Farallon Plate.

643
644 In our model for closure of the Slide Mountain Ocean we implement diachronous collision of the
645 Eastern Klamath, Yukon-Tanana, Quesnellia and Stikinia terranes with North America from 260 to 230
646 Ma, such that the southern and narrowest part of the ocean closes first (Figure 4). The Eastern
647 Klamath Terrane begins colliding with North America at 260 Ma, with final suturing at 240 Ma. The
648 initial collision of the Yukon-Tanana, Stikinia and Quesnellia terranes begins later at 250 Ma, in the
649 south, with final suturing at 230 Ma. These initial terrane collisions are associated with the roughly
650 synchronous (Beranek and Mortensen, 2011) latest Permian–Early Triassic Sonoma Orogeny
651 described in the western United States (Wyld, 1991; Dickinson, 2004; Dickinson, 2006) and the
652 Klondike Orogeny described further north in the Canadian Cordillera (Beranek and Mortensen, 2011).
653 Both orogenies have been attributed to terrane amalgamation and Slide Mountain Ocean closure in the
654 Permo-Triassic (e.g. Dickinson, 2006; Nelson et al., 2006; Colpron and Nelson, 2009; Beranek and
655 Mortensen, 2011). We model the commencement of east-dipping subduction of the Farallon Plate
656 beneath the amalgamating terranes, and subsequently North America, in response to their initial

657 collision. Therefore we initiate east-dipping subduction beneath the East Klamath portion of the
658 growing North American margin at 260 Ma, and beneath the Yukon-Tanana portion of the margin at
659 250 Ma. These Permo-Triassic timings coincide with earliest pluton emplacement in the western
660 North America Cordillera (e.g. Barth et al., 1997), with recent dating of arc plutons in the Sierra region
661 (East Klamath block in reconstruction model) constraining initial emplacement to between 256 and
662 240 Ma (Saleeby and Dunne, 2015). East-dipping subduction initiation outboard of the East Klamath
663 section of the North American margin is also consistent with the work of Saleeby (2011) who
664 proposed a ~255 Ma age based on Sm-Nd dating of a Kaweah Serpentinite Mélange garnet amphibolite
665 (southern part of East Klamath block in reconstruction model).

666

667 During the 270–230 Ma closure of the Slide Mountain Ocean, the Alexander and Wrangellia terranes
668 remain in the interior of Panthalassa and the Alexander Ocean slowly starts to obliquely subduct
669 beneath Laurasia. Northeast-dipping subduction of the Farallon Plate beneath the terranes continues
670 throughout this 40 Myr timeframe.

671

672 Coinciding with final Slide Mountain Ocean closure at 230 Ma we implement a major reorganisation of
673 eastern Panthalassic plate boundaries after the model of Shephard et al. (2013). At this time opening
674 of the Alexander Ocean ceases and there is a subduction polarity reversal across the Alexander and
675 Wrangellia terranes. This polarity reversal is largely model-dependent to allow for the transition from
676 the model of Colpron and Nelson (2009) that ends in the late Paleozoic to that of Shephard et al.
677 (2013) for post 230 Ma, yet is consistent with geological observations to support arc activity during
678 the Triassic associated with subduction of the Cache Creek Ocean along the eastern margin of
679 Wrangellia (Nockleberg et al., 2000; Shephard et al., 2013). This newly formed southwest dipping
680 subduction zone extends southeastward from the Wrangellia Terrane to the western North American
681 margin (Shephard et al., 2013), along which we model subduction initiation from 260–250 Ma. In the
682 model of Shephard et al. (2013) the ocean basin that existed between western North America and the
683 Alexander and Wrangellia terranes at 230 Ma is referred to as the Cache Creek Ocean, and based on
684 our reconstruction this ocean basin comprised crust from the Alexander Ocean and Farallon Plate that

685 was trapped during the reorganisation (Figure 4). As in the model of Shephard et al. (2013) the Cache
686 Creek Ocean is subducted contemporaneously beneath North America, and the Alexander and
687 Wrangellia terranes. We implement a transform margin along the northern Cache Creek Ocean to
688 accommodate its closure, whereby exploiting the former northern boundary of the Alexander Ocean.
689

690 We model initial collision of the Wrangellia and Alexander terranes with western North America at
691 180 Ma, in the Early Jurassic. The timing of amalgamation is a matter of ongoing debate and we favor a
692 latest Triassic to mid Jurassic collision (McClelland and Gehrels, 1990; van der Heyden, 1992; Saleeby,
693 2000; Gehrels, 2001; Amato et al., 2007), rather than Cretaceous collision (Crawford et al., 1987;
694 Nokleberg et al., 2000; Trop et al., 2002; Seton et al., 2012; Shephard et al., 2013). The Moffat Volcanics
695 from the Chatham Sound region near Alaska overlie both the Alexander Terrane and Yukon-Tanana
696 Terrane, that latter of which formed the western margin of North America following its Triassic
697 accretion (Gehrels, 2001). The volcanics have been dated at 177 ± 4 Ma (U-Pb age of a metarhyolite)
698 indicating that at this time the two terranes were in close proximity, and that the Alexander Terrane
699 accreted prior to the mid Jurassic (Gehrels, 2001). At a similar time to eruption of the Moffat Volcanics,
700 metamorphism is recorded in the Tlikakila Complex of the Talkeetna Arc at 177 Ma ($^{40}\text{Ar}/^{39}\text{Ar}$ age of 3
701 metapelite samples) and the main phase of arc activity ends at 180 Ma (Amato et al., 2007). The
702 Talkeetna Arc forms part of the Peninsular Terrane that lies outboard of the Wrangellia Terrane.
703 Amato et al. (2007) suggests that the initial collision of the Talkeetna Arc with North America and
704 closure of the intervening ocean is a likely mechanism to account for the metamorphic event and the
705 change in Talkeetna Arc activity. Collision at this time is also preferred from a geodynamic
706 perspective. Terrane collision is a key trigger of subduction zone reorganisations such as polarity
707 reversals, and at about 180 Ma a polarity reversal across the Alexander and Wrangellia terranes
708 occurs, from southwest-dipping to northeast-dipping subduction (Trop et al., 2002; Trop and Ridgway,
709 2007; Gehrels et al., 2009; Shephard et al., 2013), such that subduction of the Farallon Plate
710 commences. This scenario also removes the need to invoke trench advance of several thousand
711 kilometers during closure of the Cache Creek Ocean, which results from implementing a northeast
712 dipping subduction zone along the western margin of the Alexander and Wrangellia terranes during

713 their approach towards North America. As noted by Shephard et al. (2013), in contrast to trench-
714 rollback, modelling extensive trench advance is not preferable based on observed present-day plate
715 boundary behavior (Schellart et al., 2008).

716

717 After the collision of the Alexander and Wrangellia terranes with North America at 180 Ma and
718 subsequent subduction polarity reversal, we model a period of left-lateral transtension followed by
719 left-lateral transpression between 170 and 140 Ma to represent the history of the Gravina Basin
720 (Figure 4), not previously included in model M16. The Gravina Basin formed behind the 'Insular'
721 terranes (Alexander, Wrangellia and Peninsular terranes) and its strata range in age from Late Jurassic
722 to Early Cretaceous (e.g. Berg et al., 1972; McClelland et al., 1992; Kapp and Gehrels, 1998). Our
723 preliminary model for the opening and closure of the Gravina Basin is based on the work of Kapp and
724 Gehrels (1998), who analysed detrital zircons to test five published alternative models for the
725 evolution of the basin (see also Gehrels, 2001). Our model is most similar to their Model 2 and Model 4
726 (after Monger et al., 1994), both of which are consistent with the detrital zircon records (Figure 7b and
727 d from Kapp and Gehrels, 1998). We model the Gravina Basin as a narrow rift basin that evolved in a
728 back-arc setting associated with sinistral motion (see also Monger et al., 1994), without progressing to
729 seafloor spreading. We implement a cessation of Gravina Basin relative motions in the Early
730 Cretaceous (140 Ma), and suggest that future work should extend the model to incorporate the history
731 of mid Cretaceous thrust faulting that is recorded in the basin (Gehrels et al., 1992).

732

733 Incorporating detailed regional complexities, such as proposed oroclinal enclosure of the Cache Creek
734 Ocean (Mihalynuk et al., 1994; Mihalynuk et al., 2004), are beyond the scope of this model and are
735 suggested for future model refinements. Furthermore, our updated model for western North America
736 Mesozoic accretion events does not extend south along the western United States margin. Late Jurassic
737 arc-arc accretion outboard of the continent has been described between 159–154 Ma in the Blue
738 Mountain Province of Oregon (e.g. Schwartz et al., 2011; Johnson et al., 2015) and this event was
739 recently linked with the 154–150 Ma Nevadan Orogeny further south in the Klamath Mountains

740 (Johnson et al., 2015). These diachronous collision events, that may have been geodynamically linked
741 (Johnson et al., 2015), should also be incorporated in future model iterations.

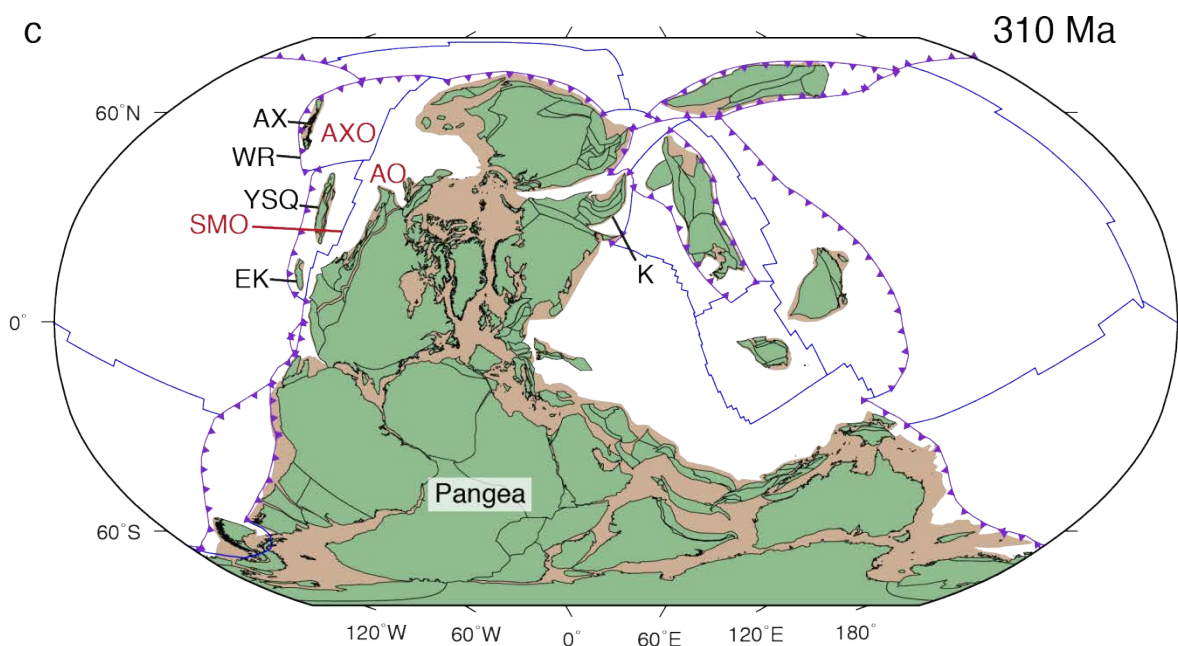
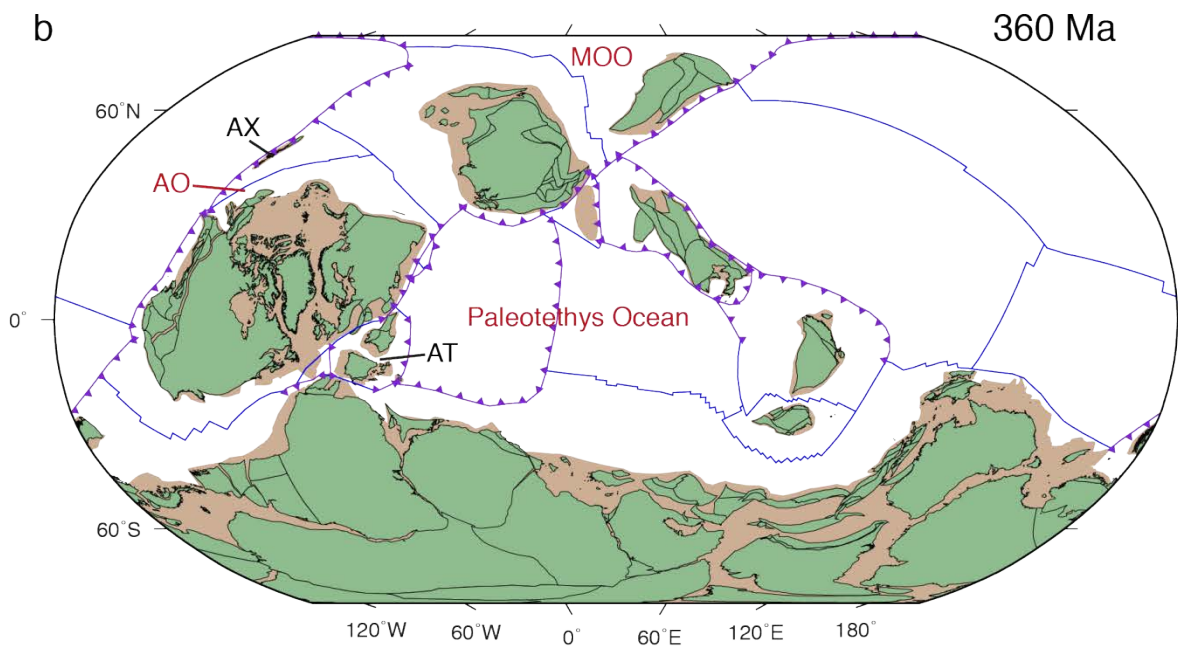
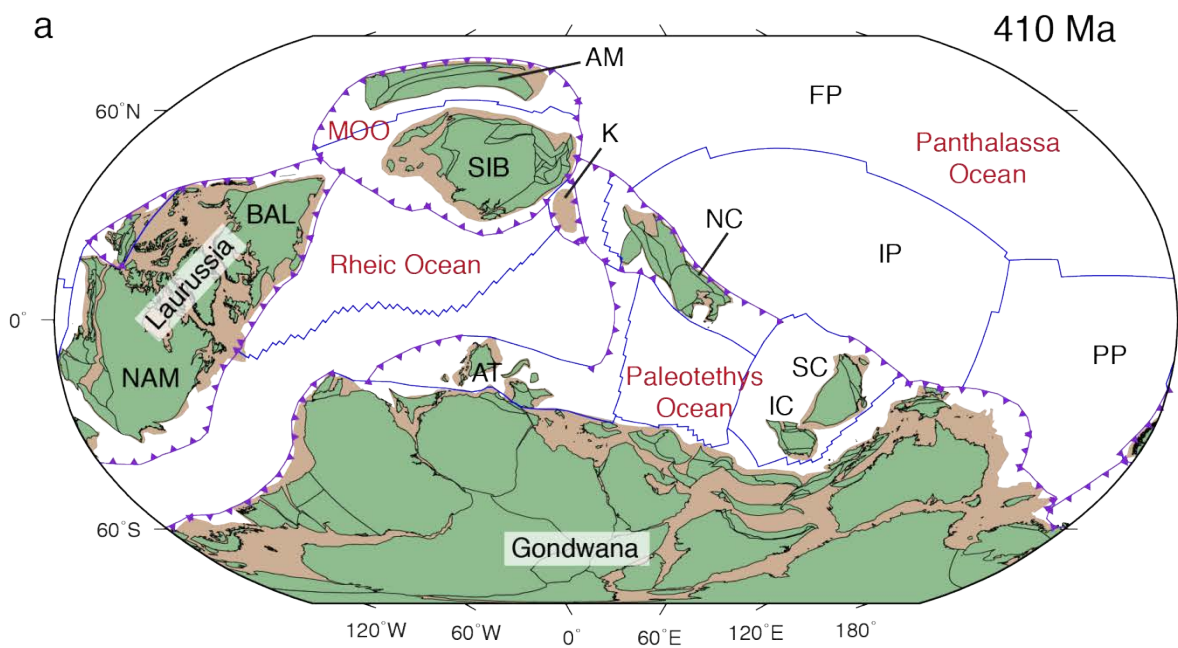
742

743 **4 Global plate motions since 410 Ma**

744

745 A number of global snapshots from the continuous 410–0 Ma plate model are shown in Figure 5 (also
746 see Supplementary Animation S2). The 410–250 Ma and 230–0 Ma global reconstructions are
747 described in detail in Domeier and Torsvik (2014) and Müller et al. (2016), and the updated evolution
748 of western North America from 410–140 Ma is described above in Section 3. Here we present a brief
749 summary of the major tectonic events including ocean basin formation and destruction and major
750 continental amalgamation and dispersal events.

751



753 **Figure 5**

754 Global 410-0 Ma plate reconstruction at roughly 50 Myr intervals, with an additional reconstruction at 230 Ma,
755 during the model transition period. Major plates (black labels) and oceans (red labels) are identified, as well as
756 smaller ones described in text. Several continent amalgamations are also identified as a guide. See text for a
757 summary of key tectonic events. Present-day coastlines are shaded green and an approximation for the extent of
758 the continents is shaded brown (modified from Müller et al., 2016 for times older than 230 Ma). AkP, Aluk Plate;
759 AM, Amuria; AO, Angayucham Ocean; AP, Antarctic Plate; AT, Armorican terranes; AX, Alexander Terrane; AXO,
760 Alexander Ocean; BAL, Baltica; CAO, Central Atlantic Ocean; CbP, Caribbean Plate; CCO, Cache Creek Ocean; CP,
761 Cocos Plate; CtP, Catequil Plate; CzP, Chazca Plate; EK, Eastern Klamath Terrane; FP, Farallon Plate; GB, Gravina
762 Basin; HP, Hikurangi Plate; IC, Indochina; IP, Izanagi Plate; K, Kazakhstan; KLA, Kohistan-Ladakh Arc; KLB,
763 Kohistan-Ladakh back-arc basin; KP, Kula Plate; MOO, Mongol-Okhotsk Ocean; MP, Manihiki Plate; MTO,
764 Mesotethys Ocean; NAM, North America; NC, North China; NP, Nazca Plate; NTO, Neotethys Ocean; PcP, Pacific
765 Plate; PD, Pontides Terrane; PP, Phoenix Plate; PS, Philippine Sea; PSCS, Proto South China Sea; PTO, Paleotethys
766 Ocean; SAO, South Atlantic Ocean; SC, South China; SIB, Siberia; SMO, Slide Mountain Ocean; VP, Vancouver Plate;
767 WA, Woyla Arc; WB, Woyla back-arc basin; WR, Wrangellia Terrane; YSQ, Yukon-Tanana, Stikinia and Quesnellia
768 terranes.

769

770 At 410 Ma (Figure 5a), the commencement of the model in the Devonian, Gondwana is located in
771 southerly latitudes with southern Africa and Antarctica located at the South Pole. At this time the
772 Variscan terranes, Indochina and South China have already rifted from Gondwana and their motion is
773 associated with the growth of the Paleotethys Ocean off the African-Indian-Australian margin.
774 Gondwana is separated from Laurussia and Siberia by the closing Rheic Ocean, which is surrounded by
775 subduction zones. The largest ocean at this time, and for the duration of the model, is Panthalassa
776 (later forming the Pacific Ocean). Panthalassa borders the Australian margin of Gondwana and
777 dominates almost an entire hemisphere. Opening of the Mongol-Okhotsk Ocean between Siberia and
778 Amuria is already underway when the model commences.

779

780 Over the course of the Devonian the Rheic Ocean is consumed, resulting in the eventual amalgamation
781 of Laurussia, the Variscan terranes and Gondwana. North America (part of Laurussia) initially collides
782 with the western margin of South America (part of Gondwana) at 380 Ma, before immediately rifting

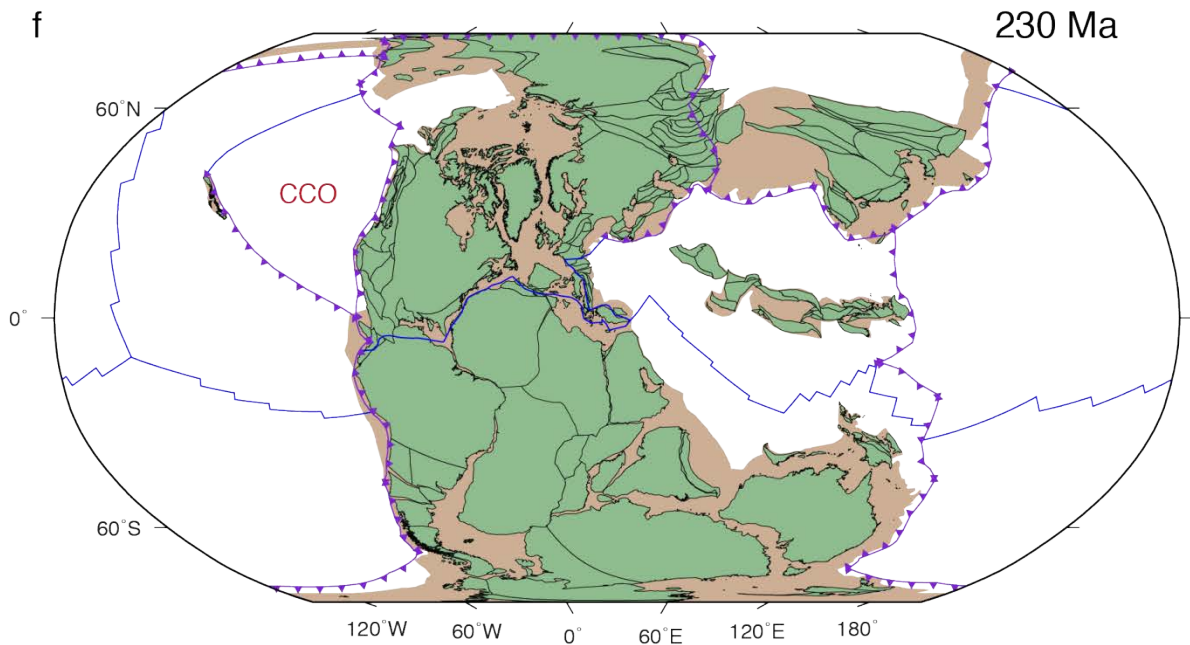
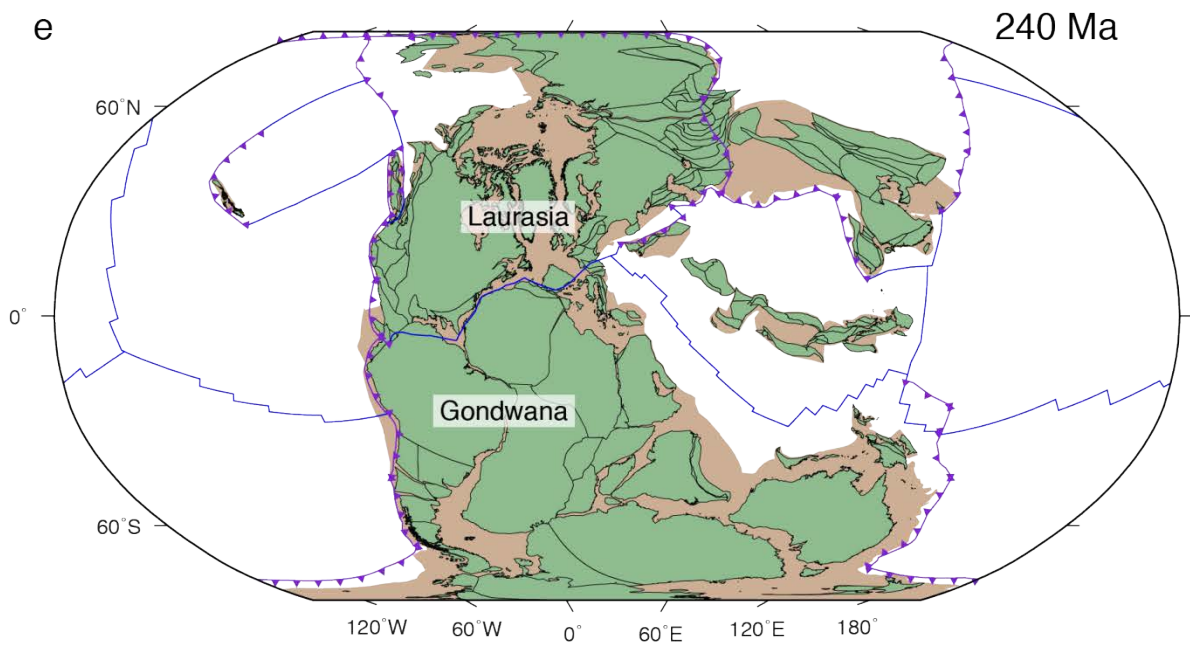
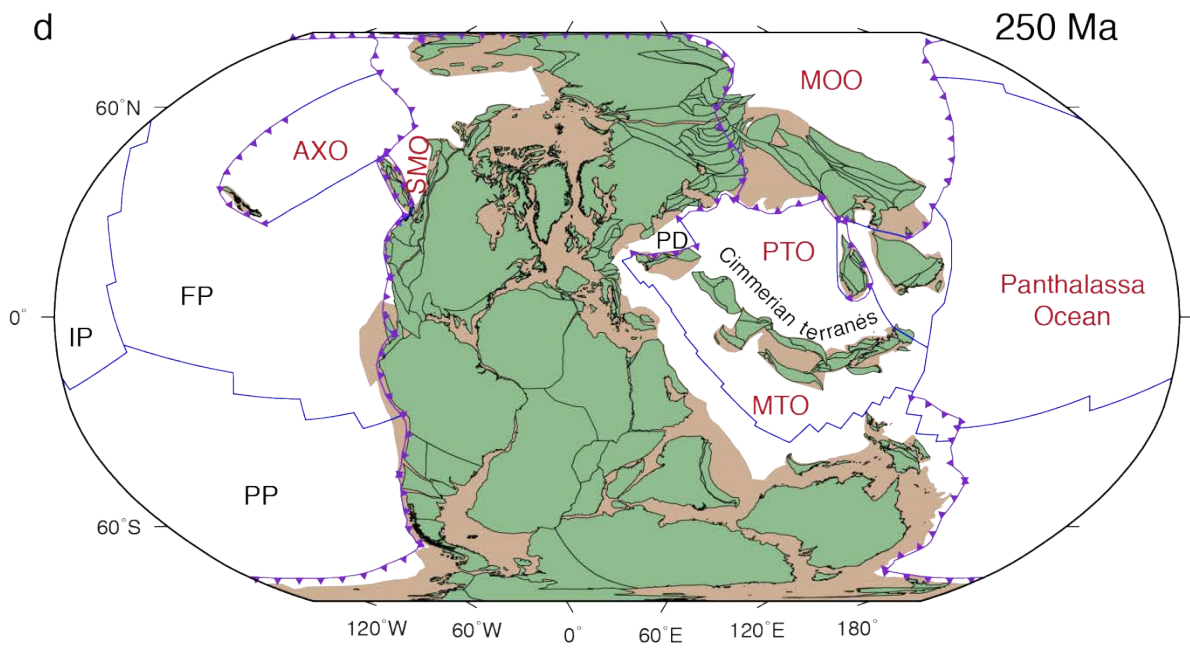
783 away and migrating towards its Pangea position via mainly transform motion. Throughout this time an
784 ocean begins to open between Laurussia and Siberia, while the Mongol-Okhotsk Ocean begins to
785 subduct beneath Siberia (360 Ma), although spreading between Siberia and Amuria is ongoing
786 throughout the entire Paleozoic. Subduction zone rollback triggers the detachment of the Alexander
787 Terrane from northern Baltica, leading to a major back-arc basin forming event (Figure 5b). As the
788 Alexander Terrane migrates towards Panthalassa, back-arc rifting propagates southward along the
789 western North American margin in the late Devonian resulting in the opening of the Slide Mountain
790 Ocean behind the Yukon-Tanana, Stikinia, Quesnellia and East Klamath terranes (Figure 5c).
791 Throughout this timeframe seafloor spreading continues in the Paleotethys, and Indochina and South
792 China remain isolated from Gondwana.

793
794 During the Carboniferous, convergence between Laurussia and Siberia leads to closure of the
795 intervening ocean and their amalgamation at 320 Ma, and ultimately ends in the formation of Pangea.
796 Subduction of the Mongol-Okhotsk Ocean beneath Siberia continues throughout the Carboniferous,
797 and at 330 Ma it also begins subducting beneath Amuria. Spreading continues in the Paleotethys, while
798 it is consumed by subduction along its western and northern margins. A major event during this
799 period is rifting of the Cimmerian terranes (Figure 5d) from northern Gondwana in the Permian, with
800 their separation at 275 Ma. This results in the opening of the Mesotethys Ocean to their south. In
801 Panthalassa the Slide Mountain Ocean and its northern continuation behind the Alexander Terrane
802 (Alexander Ocean) continue opening until a plate boundary reorganisation in the Permian at 270 Ma.
803 At this time the Slide Mountain Ocean begins to close following a subduction polarity reversal across
804 the Yukon-Tanana, Stikinia, Quesnellia and East Klamath terranes. The Alexander and Wrangellia
805 terranes continue their Panthalassic migration during Slide Mountain Ocean closure.

806
807 At 250 Ma (Figure 5d), the earliest Triassic and beginning of the Mesozoic, Amuria collides with North
808 China and subduction of the Mongol-Okhotsk Ocean beneath Amuria ceases. At 230 Ma (Figure 5f)
809 another major plate boundary reorganisation in Panthalassa results in a subduction polarity reversal
810 across the Alexander and Wrangellia terranes and the initiation of contemporaneous subduction along

811 western North America. During the Jurassic, suturing of the Cimmerian terranes to southern Eurasia,
812 and thus final closure of the Paleotethys, leads to a southward jump of the north-dipping subduction
813 zone to consume the Mesotethys. Final closure of the Mongol-Okhotsk Ocean also occurs in the
814 Jurassic, as does the collision of the Alexander and Wrangellia terranes with western North America
815 and the birth of the Pacific Plate at the Farallon-Izanagi-Phoenix spreading ridge triple junction
816 (Figure 5h).

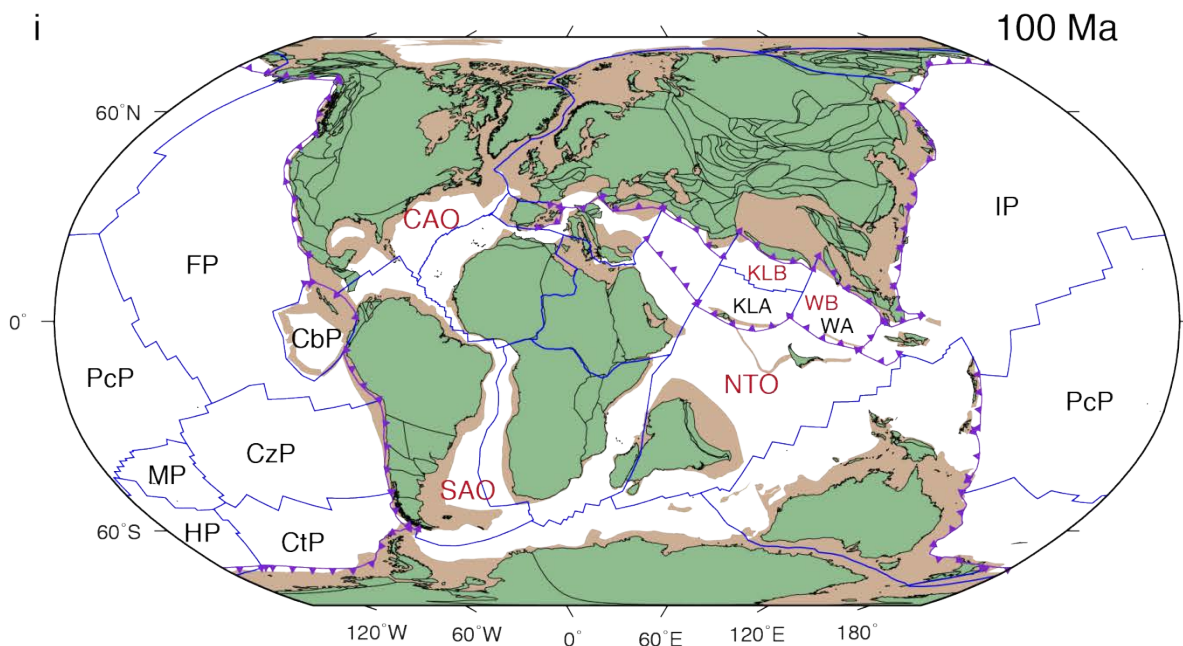
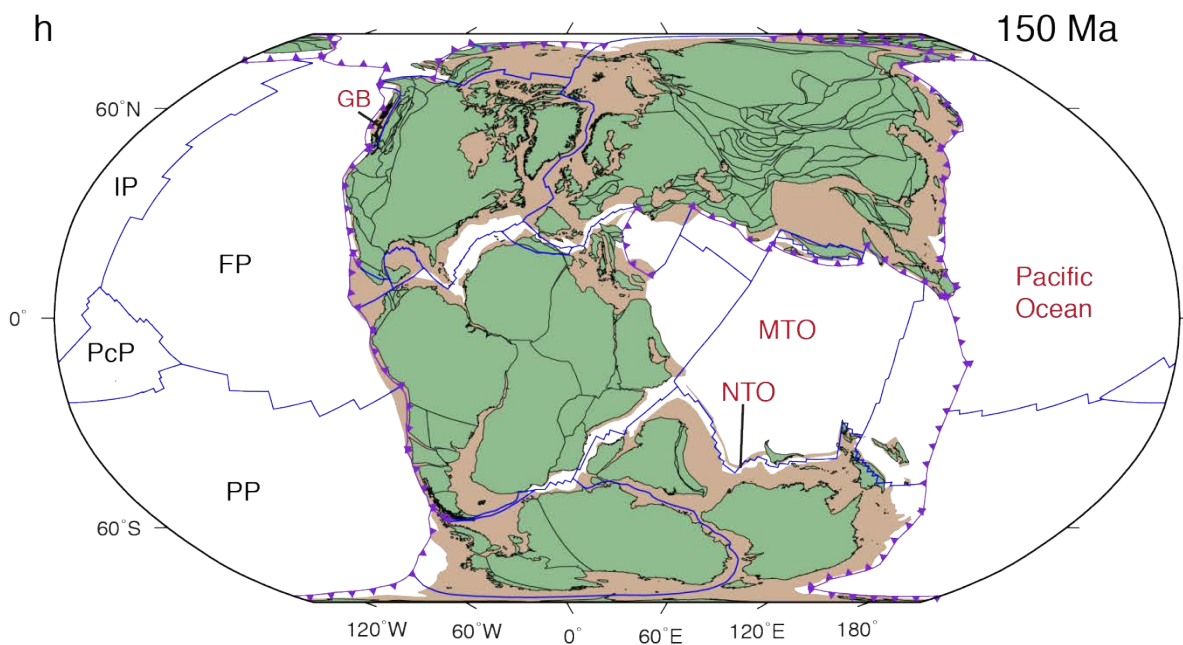
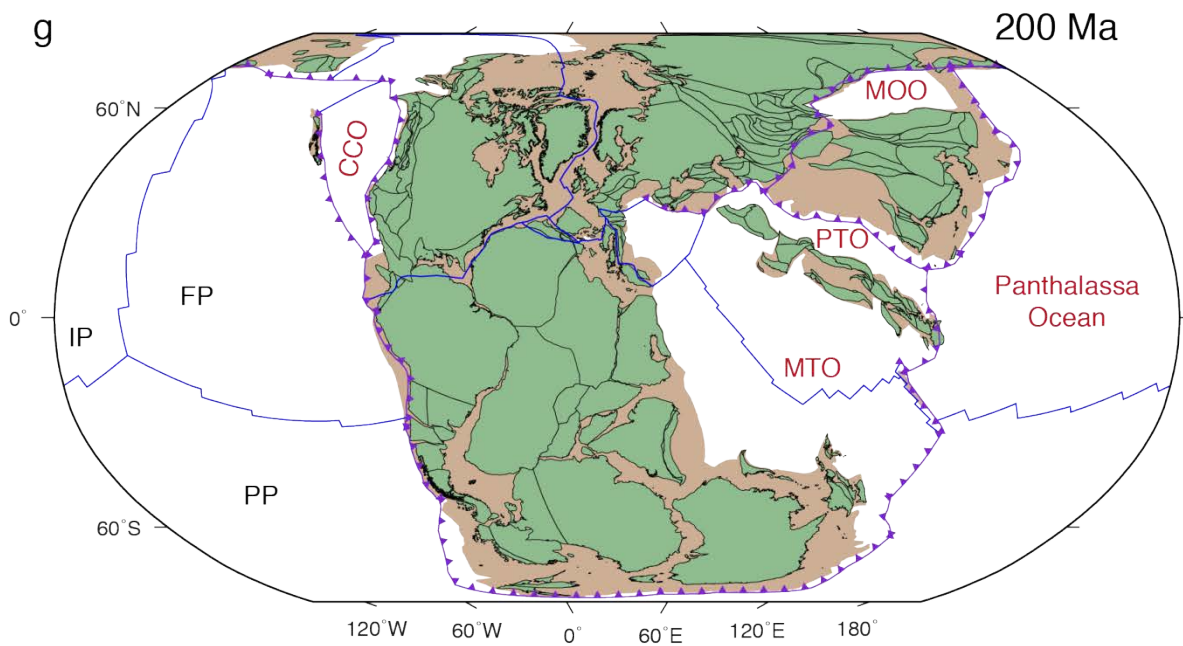
817



819 **Figure 5.** Continued.

820

821 By the latest Jurassic (Figure 5h) Pangea breakup is well underway and continental fragments rift
822 from Gondwana associated with opening of the Neotethys Ocean, contemporaneous with back-arc
823 basin opening along southern Eurasia. Whilst spreading in the Central Atlantic and between Africa and
824 Madagascar begins in the Jurassic, the Cretaceous sees the opening of the South Atlantic and opening
825 of central and eastern Indian Ocean due to separation of India from Antarctica and Australia. A major
826 plate reorganisation event in the Pacific occurs at 120 Ma with fragmentation of the Phoenix Plate
827 triggered by eruption of the Ontong-Java-Manihiki-Hikurangi large igneous province (see Seton et al.,
828 2012 for an in-depth description of this part of the model). This event results in the birth of the
829 Hikurangi, Manihiki, Catequil and Chazca oceanic plates (Seton et al., 2012).



831 **Figure 5.** Continued

832

833 A key feature of the Late Cretaceous to present-day timeframe (Figures 5i-k) is the myriad of back-arc
834 basin formation and destruction events in the western Pacific, Southeast Asia and the Southwest
835 Pacific. In the Indian Ocean, India collides with the intra-oceanic Kohistan-Ladakh Arc at ~52 Ma, and
836 the India-Eurasia continent-continent collision initiates at ~47–43 Ma. During this time there is also
837 separation of Greenland from both North America and Europe, associated with opening of both the
838 Labrador Sea, which ceased at 32 Ma, and the North Atlantic, which continues to widen at present-day.
839 In the Pacific, the Izanagi Plate is fully subducted beneath Eurasia, while the Farallon Plate
840 sequentially fragments to form the Kula, Vancouver, Juan de Fuca, Nazca and Cocos plates through the
841 Late Cretaceous and Cenozoic.

842

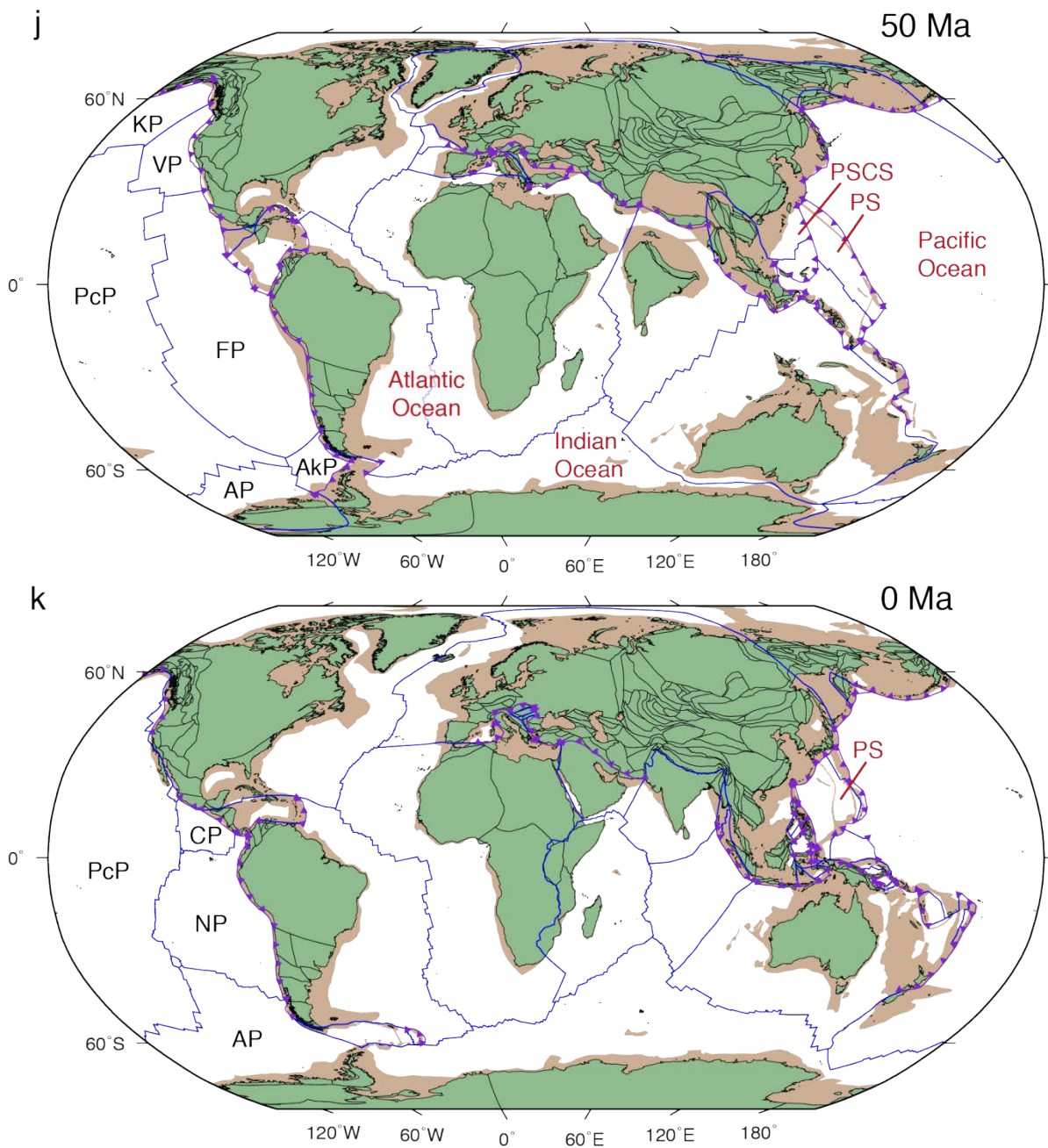


Figure 5. Continued.

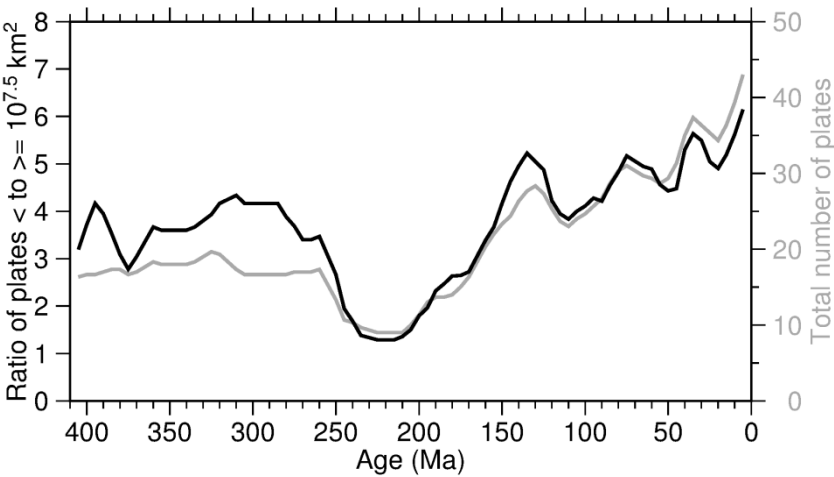
5 Model analysis and discussion

Now we look at some of the geodynamic characteristics of our model from 410 Ma to present-day, to see whether these characteristics change or remain consistent over the entire timeframe. Namely we consider the number of plates and their size distribution through time, global continental and plate

850 RMS speeds, plate velocities, and trench migration patterns. These results are also intended to
851 highlight potential regions and times for future model testing and refinement.

853 **5.1 Number of plates**

854 The number of plates modelled since 410 Ma ranges from 9 to 45. Major first-order trends include
855 higher numbers of plates during the past 150 Myr compared to earlier times, and a noticeable dip in
856 the total number of plates from 260–160 Ma, such that from ~230–205 Ma there are only 9 plates
857 (Figure 6). Both of these trends are at least partially attributed to a lack of seafloor preservation and
858 difficulty in modelling small plates prior to the Cenozoic (Mallard et al., 2016).



859
860 **Figure 6**
861 Total number of plates (grey line) and the ratio of plates smaller than $10^{7.5} \text{ km}^2$ to “large” plates ($\geq 10^{7.5} \text{ km}^2$)
862 (black line) through time. Values are extracted at 5 Myr intervals and then plotted as 10 Myr moving averages.

863
864 The latest Paleozoic–early Mesozoic timeframe (260–160 Ma) is of particular importance in the model
865 as it encompasses the evolution of the assembled supercontinent Pangea through the start of breakup,
866 and, in technical terms, also includes the model transition period (250–230 Ma) and the latest
867 extension (230–200 Ma) to the global Mesozoic model described by Müller et al. (2016). As a result,
868 250–200 Ma in particular has received less regional refinement compared to older and younger times.
869 This trend of a major reduction to the number of plates during a time of supercontinent fragmentation
870 therefore suggests that model refinement is needed, particularly from 260 to 160 Ma, to capture more

871 regional complexities, such as the evolution of smaller continents and back-arc or marginal basins.
872 Prior to this potentially anomalous 260–160 Ma timeframe, there are around 16–20 plates from 410 to
873 260 Ma. While a reduction in the number of plates, compared to present-day, is expected due to an
874 absence of preserved seafloor to constrain the plate model, fewer plates may also be expected during
875 Pangea assembly and growth as continents are amalgamating and ocean basins are being destroyed.

876

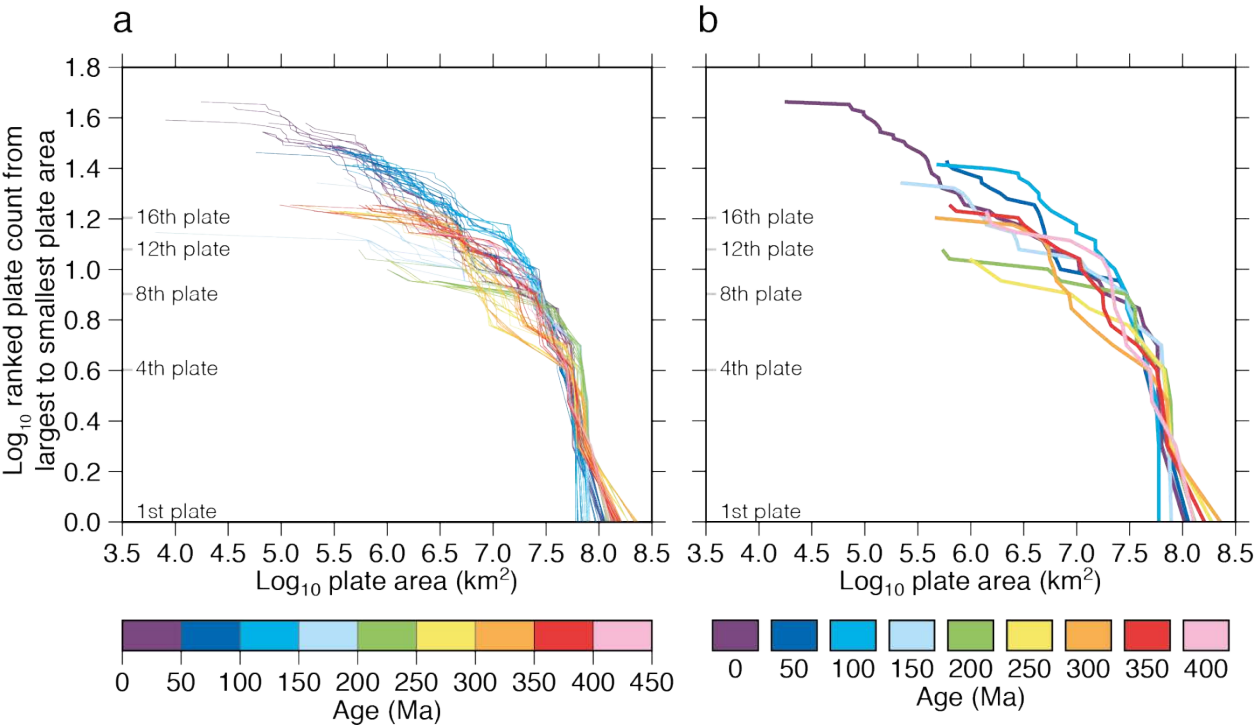
877 5.2 Plate size through time

878

879 Morra et al. (2012) analysed the size distribution of plates over the past 200 Myr (using the
880 reconstruction of Seton et al., 2012), and patterns in the standard deviation of plate size for the largest
881 six, seven and eight plates. In agreement with the findings of Bird (2003) for the present-day, they
882 found a robust distinction between large and small plates since 200 Ma. There are consistently few,
883 ~8, “large” plates ($\geq 10^{7.5}$ km² or $\sim 32 \times 10^6$ km²) and many smaller plates. Furthermore, over the past
884 60 Myr, the timeframe considered most reliable for small basin reconstruction, the distribution of the
885 smaller plates follows a power law distribution (Morra et al., 2012), also noted by Bird (2003) for
886 present-day. When analysing the standard deviation of plate size for the six, seven and eight largest
887 plates Morra et al. (2012) found that since Gondwana breakup, the plate system moves rapidly
888 towards a large standard deviation in plate size (i.e. one dominant plate), which they refer to as
889 “heterogeneous tessellation”, whilst there is a “slow relaxation” towards a low standard deviation in
890 plate size, referred to as “homogeneous tessellation”. They further suggested a 100 Myr cycle between
891 heterogeneous and homogeneous tessellation, with the inflection points coinciding with global plate
892 reorganisation events. For instance the well-recognized plate reorganisation at ~50 Ma (Gordon and
893 Jurdy, 1986; Whittaker et al., 2007) coincides with a change from increasing to decreasing standard
894 deviation in plate size, while the 100 Ma reorganisation (Veevers, 2000; Matthews et al., 2012)
895 coincides with a change from decreasing to increasing size. Here, we analysed the plate size
896 distributions of our model to determine if similar trends to those described by Morra et al. (2012)
897 have persisted since the late Paleozoic, and hence during an entire supercontinent cycle.

898

899 From 160 Ma to present-day there are ~5–8 large plates ($\geq 10^{7.5}$ km²) (Figure 7) and ~3.7–6.6 times as
 900 many smaller plates, that is, with areas $< 10^{7.5}$ km² (Figures 6). During this timeframe we see the most
 901 similarity with the results of Morra et al. (2012) in terms of the numbers of large plates. For times
 902 older than 160 Ma the characteristic distribution is slightly different, with 4–6 large plates and a ratio
 903 of small to large plates of ~1.3–4.5 (Figures 6). If we exclude the 260 to 160 Ma timeframe, for which
 904 there is a major, potentially artificial drop in the number of plates (see previous section, Section 5.1),
 905 then there are still 4–6 large plates from 410–260 Ma, however the ratio of small to large plates
 906 becomes ~2.7–4.5. This decreased ratio of small to large plates, compared to present-day and more
 907 recent times, likely reflects the lack of seafloor preservation and the difficulty in reconstructing
 908 smaller plates (Mallard et al., 2016). Consistently throughout the model there are fewer large plates
 909 compared to smaller plates, as seen at present-day, however a decrease in the number of large plates
 910 during the late Paleozoic may be consistent with the growth of a single large plate (i.e. comprising
 911 Pangea).



912
 913 **Figure 7**
 914 The logarithms of plate size versus cumulative plate count for the global model (after Morra et al., 2012). Large
 915 plates are considered to be $\geq 10^{7.5}$ km² in area, that is, with a value ≥ 7.5 on the x-axis (Morra et al., 2012). To a
 916 first order, throughout the model there tends to be few large plates and many smaller plates. From ~250-200 Ma

917 (green), however, there are very few plates, particularly plates smaller than $10^{7.5}$ km², and thus the trend is less
918 distinct. (a) Results plotted every 5 Myr. (b) Results plotted every 50 Myr.

919

920 When we look at the trends of the largest six, seven and eight plates since the late Paleozoic (Figure 8)
921 there are two main differences to those discussed by Morra et al. (2012) that likely reflect the
922 inclusion of final Pangea assembly and initial breakup, and thus highlight there are additional
923 complexities in plate tessellation patterns when considering timeframes of several hundreds of
924 millions of years. Morra et al. (2012) proposed a 100 Myr cycle between heterogeneous and
925 homogeneous tessellation, and linked the cycle to the behaviour of the oceanic plates, specifically the
926 growth of a dominant oceanic plate (Pacific Plate). At times earlier than 200 Ma, we find that the
927 trends are governed by events associated with growth and fragmentation of Pangea, which forms part
928 of a composite continental-oceanic plate, dominated by continental lithosphere. Changes to the
929 oceanic portion of the plate nonetheless play an important role in modulating its overall size,
930 particularly during final assembly and initial fragmentation (Figure 8). After extraction of a major
931 oceanic portion of the plate, in the Tethys realm, at 275 Ma, continental rifting is the dominant
932 controller of its size. Morra et al. (2012) also proposed that over the past 200 Myr the transition from
933 homogeneous to heterogeneous tessellation is rapid while the reverse occurs more slowly. We found
934 the opposite trend during the supercontinent assembly and initial breakup phase of the model (~410–
935 180 Ma). The increase in heterogeneous tessellation to a maximum at 275 Ma occurs over at least 135
936 Myr (data only available from 410 Ma), while Pangea fragmentation and the movement towards more
937 homogeneous tessellation is faster, taking only 25 or 95 Myr, depending on whether the 60 Myr
938 increase in standard deviation from 240–180 Ma is excluded or included, respectively (Figure 8).

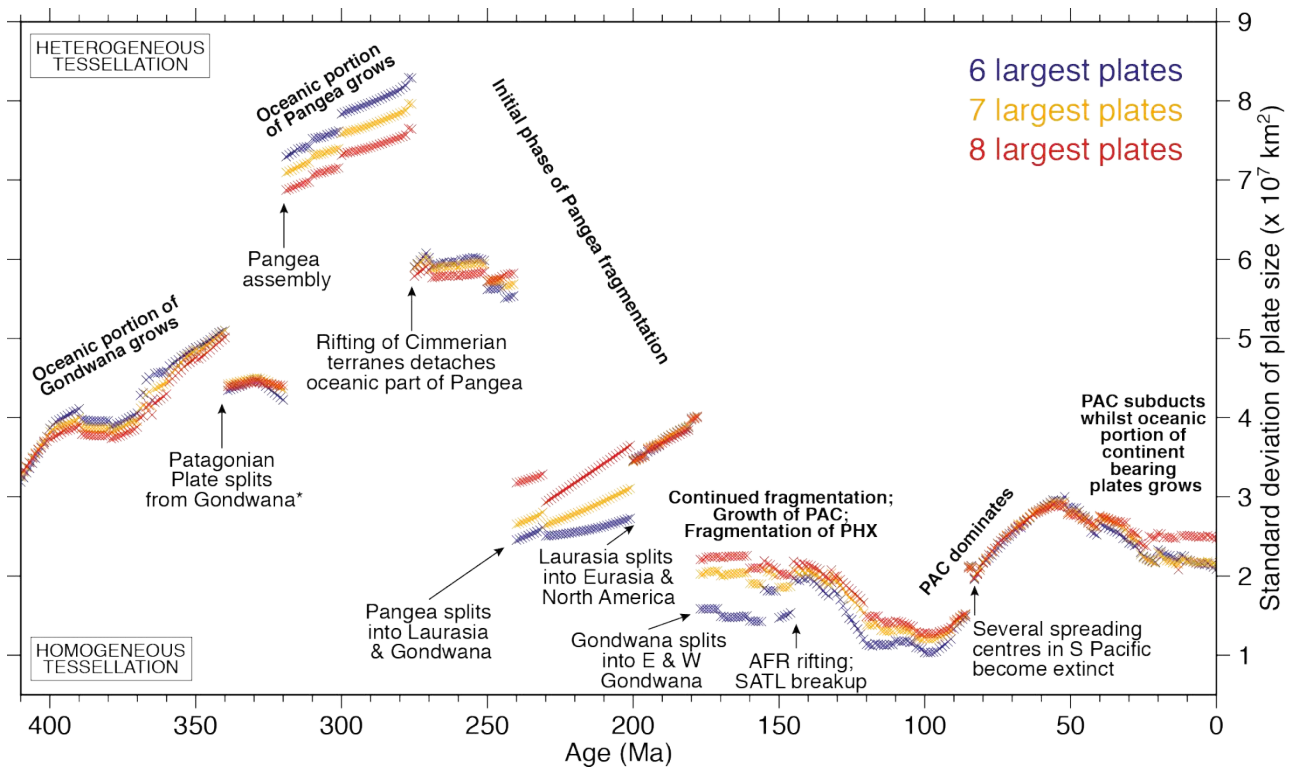


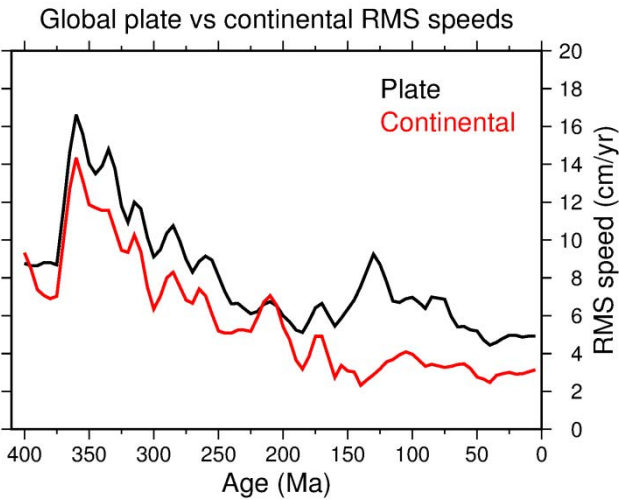
Figure 8

Standard deviation of plate size through time for the 6, 7 and 8 largest plates, plotted at 5 Myr intervals. Major tectonic events resulting in the amalgamation or fragmentation of plates are also identified. As described by Morra et al. (2012) lower standard deviation values correspond to “homogeneous tessellation” scenario (the largest plates are similar in size), while larger values correspond to a scenario of “heterogeneous tessellation” (there is one dominant plate). AFR, African Plate; PAC, Pacific Plate; PHX, Phoenix Plate; SATL, South Atlantic breakup.

5.3 Plate velocities and global RMS speeds

It has long been recognised that continents move more slowly than oceanic or composite plates (e.g. Forsyth and Uyeda, 1975; Gordon and Jurdy, 1986; Zahirovic et al., 2015). For instance, Gordon and Jurdy (1986) made this observation from studying six time instances in the Cenozoic, and more recently Zahirovic et al. (2015) analysed plate velocities from a global plate reconstruction model (Seton et al., 2012) for the past 200 Myr. Zahirovic et al. (2015) also calculated global continental RMS speeds and compared the results with whole plate RMS speeds since 200 Ma, and found that for the post-Pangea timeframe continental speeds are consistently lower at ~ 3 cm/yr (remaining below 6 cm/yr), compared to ~ 5 – 10 cm/yr for the plates, which are either partly or entirely oceanic. The only

957 exception is at 110–100 Ma when there is a spike in the counter-clockwise rotation of Africa. This
 958 trend of continents generally moving slower than whole plates is a simple benchmark against which to
 959 evaluate a global plate motion model. We thus compute these statistics for the current 410–0 Ma
 960 model using the workflow of Zahirovic et al. (2015). This work is complementary to that of Domeier
 961 and Torsvik (2014) and Müller et al. (2016) who analysed the speed of individual plates and
 962 continents in models DT14 and M16, respectively.



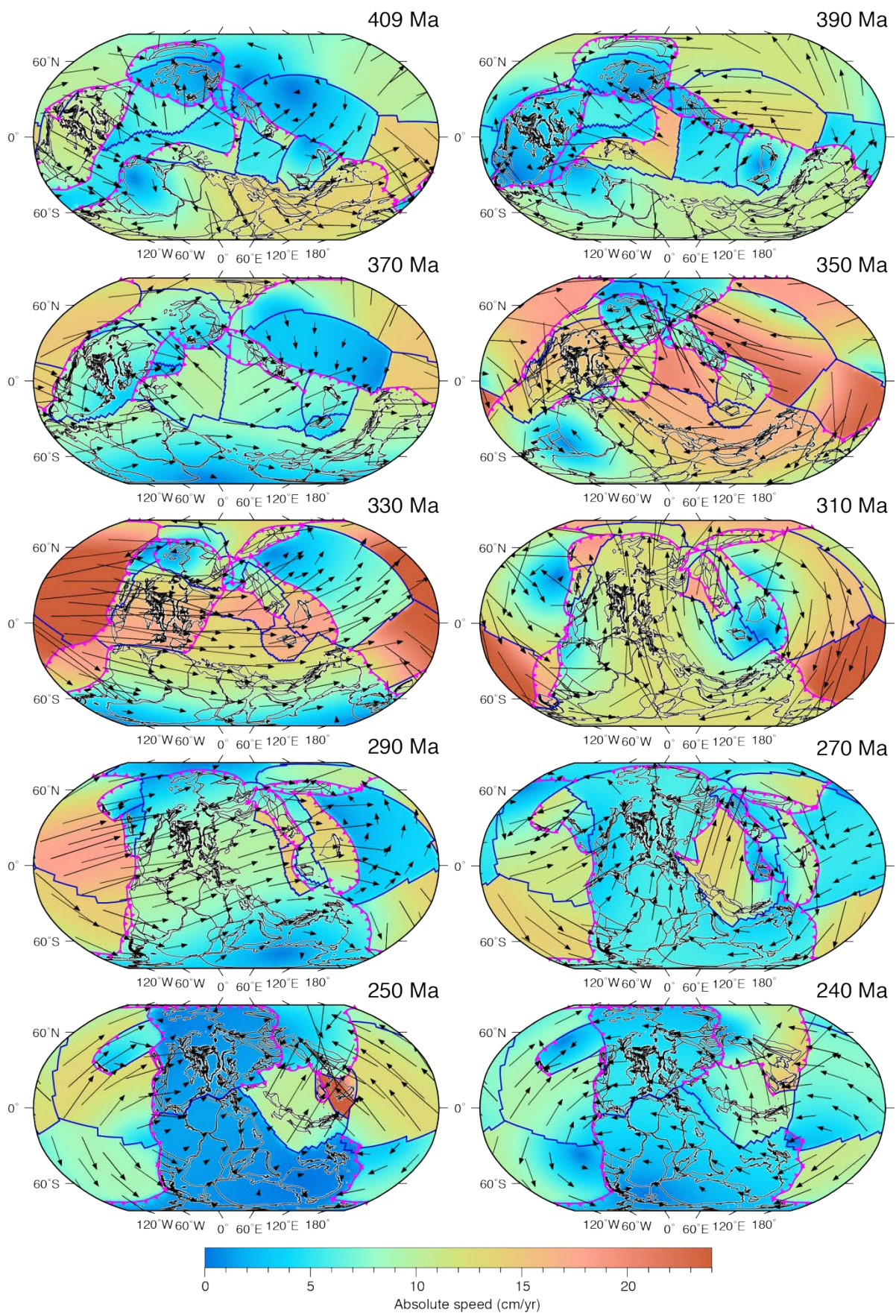
963

964 **Figure 9**

965 Global plate (black line) and continent-only (red line) RMS speeds through time. The continental curve excludes
 966 the oceanic portion of the plates. Values are extracted at 5 Myr intervals and then plotted as 10 Myr moving
 967 averages.

968

969 Continental versus plate RMS speeds for the past 410 Myr are shown in Figure 9 and global absolute
 970 plate velocities at selected times are shown in Figure 10 (also see Supplementary Animation S3). The
 971 global whole plate RMS speeds remain higher than the continental RMS speeds throughout the model,
 972 except for briefly at 220–200 Ma. This trend is therefore largely consistent with the findings of
 973 Zahirovic et al. (2015) for the past 200 Myr, including at present-day, and strongly suggests that the
 974 spike in continental RMS speeds at 220–200 Ma signifies a kinematic modelling artefact. Regarding the
 975 magnitude of motion, plate and continental RMS speeds show an overall increase moving back through
 976 time starting from ~200 Ma, reaching a peak at 365 Ma of >16 cm/yr and >14 cm/yr, respectively,
 977 after which there is a rapid decrease to ~9 cm/yr and 7 cm/yr, respectively, at 370 Ma. There is also a
 978 noticeable peak in plate RMS speeds at ~125 Ma, reaching almost 10 cm/yr.

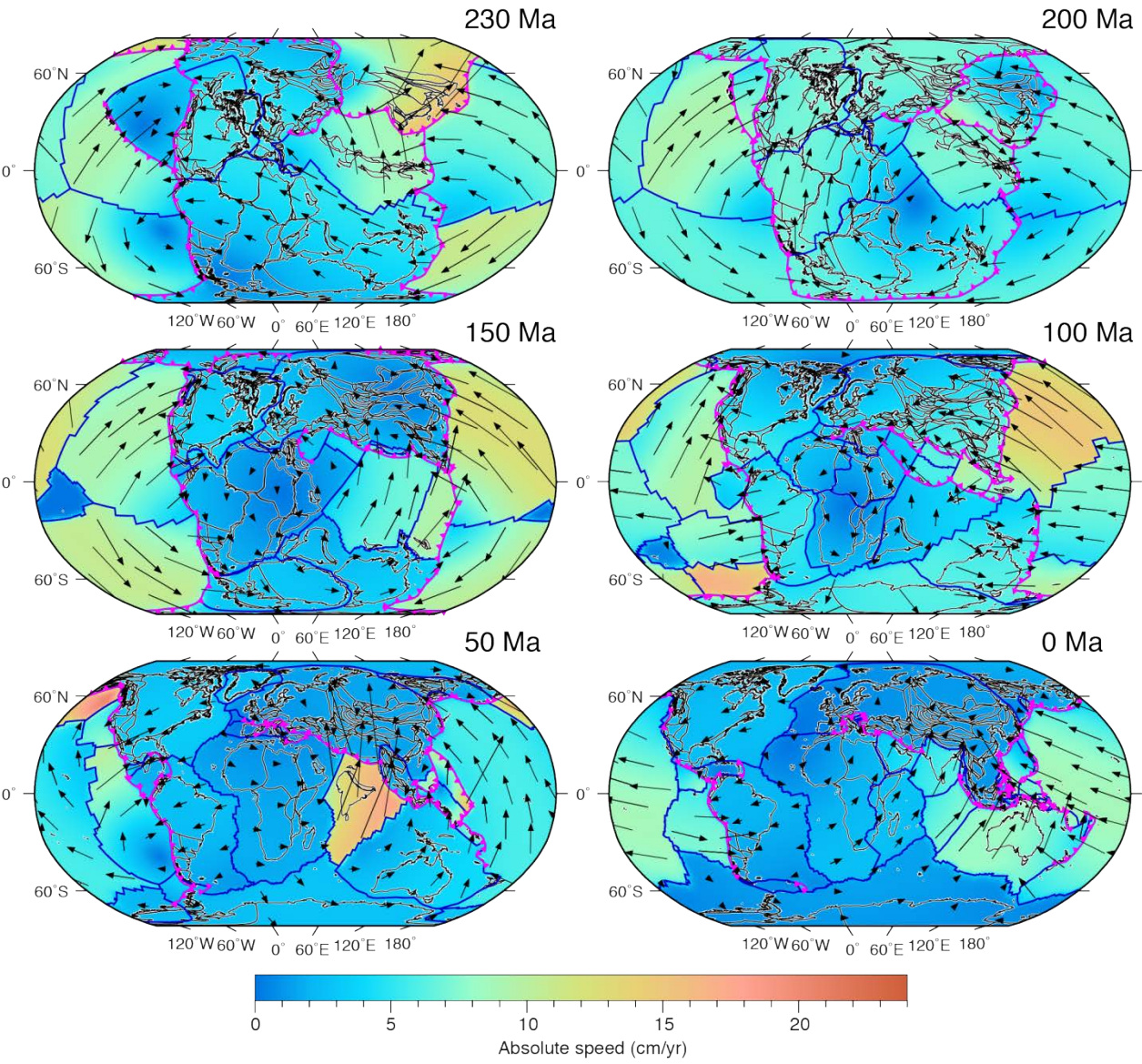


979

980

981

982 **Figure 10**
 983 Reconstructed absolute plate velocities at 10-50 Myr intervals. Fewer plots are included for the 230-0 Ma period
 984 as such an analysis was presented by Müller et al. (2016). Colours and vector lengths indicate plate speed and
 985 vector azimuths indicate absolute plate motion directions. Plate speed colouring is clipped at a maximum of 24
 986 cm/yr. Present-day coastlines (black) are also reconstructed.
 987



988
 989 **Figure 10. Continued.**
 990

991 Oceanic spreading and the motions of purely oceanic plates are synthetic during the Paleozoic and
 992 large parts of the Mesozoic, due to recycling of oceanic lithosphere into the mantle, and therefore

993 simple spreading histories are implemented, particularly in Panthalassa (Domeier and Torsvik, 2014).
994 We therefore focus our analysis on the trends in continental motions.
995
996 The above results may suggest that continental motions were faster during much of the late Paleozoic,
997 particularly during the latest Devonian and early Carboniferous, compared to the past 200 Myr.
998 Although the uncertainty in plate reconstructions increases back through time due to decreasing
999 geological constraints and preserved seafloor, these trends may not be artificial as pulses of
1000 anomalously rapid continental motion have been proposed during both the Precambrian and
1001 Phanerozoic. For example, a well-studied short (~15 Myr) burst in India's motion, of up to 18 cm/yr,
1002 occurred from ~65 Ma and has been attributed in part to effects of transient plume head arrival at the
1003 base of the lithosphere (van Hinsbergen et al., 2011) or double north-dipping subduction along and
1004 south of southern Eurasia (Jagoutz et al., 2015). Furthermore, based on paleomagnetic data, rapid
1005 continental motions (>16 cm/yr) not exceeding 50 Myr in duration have been proposed in the
1006 Precambrian and early Paleozoic for various continents including Gondwana, Laurentia and Baltica
1007 (Meert et al., 1993; Gurnis and Torsvik, 1994). However, the rapid motions of Baltica and Laurentia
1008 have also been disputed based on alternative latitude calculations from paleomagnetic data (e.g.
1009 Condie et al., 2015).
1010
1011 Alternatively, the above results may suggest that modelled continental speeds are currently
1012 unreasonably high during much of the late Paleozoic, particularly as there is such a rapid increase,
1013 with a doubling in global RMS speed, from 375 to 365 Ma. Furthermore, the fast motions do not
1014 generally seem to be restricted to any one continent, as was the case for India in the Cenozoic, and
1015 Gondwana, Laurentia and Baltica in the Precambrian/early Paleozoic (described above) (Figure 10
1016 and Supplementary Animation S3). The notable exception to this is the rapid northward motion of
1017 Indochina and South China (>20 cm/yr) between 260 and 250 Ma (Figure 10, see also Section 2.2.1.2).
1018
1019 The origin of potentially excessively high global continental RMS speeds could be rooted in the relative
1020 motion model and/or the absolute reference frame. To shed more light on high continental RMS

1021 speeds for much of the late Paleozoic, we suggest that future work should seek to confirm the trends
1022 by (1) investigating mechanisms to account for such rapid motion over >100 Myr timeframes, and
1023 during supercontinent assembly, rather than dispersal (Gurnis and Torsvik, 1994), (2) extending the
1024 plate motion model into the Precambrian to test the longevity of high continental RMS speeds, (3)
1025 testing alternative absolute reference frames, to which plate velocities are very sensitive (Shephard et
1026 al., 2012; Zahirovic et al., 2015), and (4) re-examining geological evidence for fast moving continents
1027 to determine if those constraints could also be consistent with slower speeds. Ultimately, assessing
1028 their cause requires further investigation (Domeier and Torsvik, 2014).

1029

1030 5.4 Trench migration trends

1031 Schellart et al. (2008) produced a comprehensive global compilation of present-day trench migration
1032 data, and recently Williams et al. (2015) undertook a similar analysis for the past 130 Myr. In both
1033 studies the authors compared multiple absolute reference frames. A key finding of the Schellart et al.
1034 (2008) study was that trench retreat dominates over trench advance, with ~62–78% of global trench
1035 segments (200 km in length) retreating at present-day depending on the absolute reference frame,
1036 and that the mean and median values of trench motion are therefore always positive (positive values
1037 signify retreat, while negative values signify advance) at ~1.3–1.5 cm/yr and 0.9–1.3 cm/yr,
1038 respectively. Furthermore, trench motion is modest with only 16–33% of trench segments retreating
1039 at speeds greater than 3 cm/yr and only ~1–11% advancing at speeds greater than 3 cm/yr. Williams
1040 et al. (2015) found similar results for the past 130 Ma, namely of the dominance in trench retreat over
1041 trench advance. They found a tighter distribution around 0 cm/yr for the past 70 Myr, in agreement
1042 with the preferred model of Schellart et al. (2008), and more dispersion for older times when there is
1043 less certainty in the constraints on the absolute plate motion models they tested.

1044

1045 Utilizing the workflow of Williams et al. (2015) we analysed trench migration patterns since 410 Ma.
1046 At 1 Myr intervals subduction zones were divided into 1° segments (~110 km in length at the equator)
1047 and the velocity of migration was calculated orthogonal to the trench. We consider the present-day
1048 study of Schellart et al. (2008) as a benchmark against which to compare our trench migration results

for the 410–0 Ma paleo-reconstructions. Specifically, we calculated the median value of trench motion, the percentage of trench segments retreating and advancing (these values do not necessarily add to 100% if there are stationary segments), and the percentage of segments retreating and advancing faster than 3 cm/yr (Figure 11). Additionally, the absolute positions of subduction zones through time are shown in Figure 12, indicating which regions have experienced fast or slow trench motion at different times (c.f. Collins, 2003).

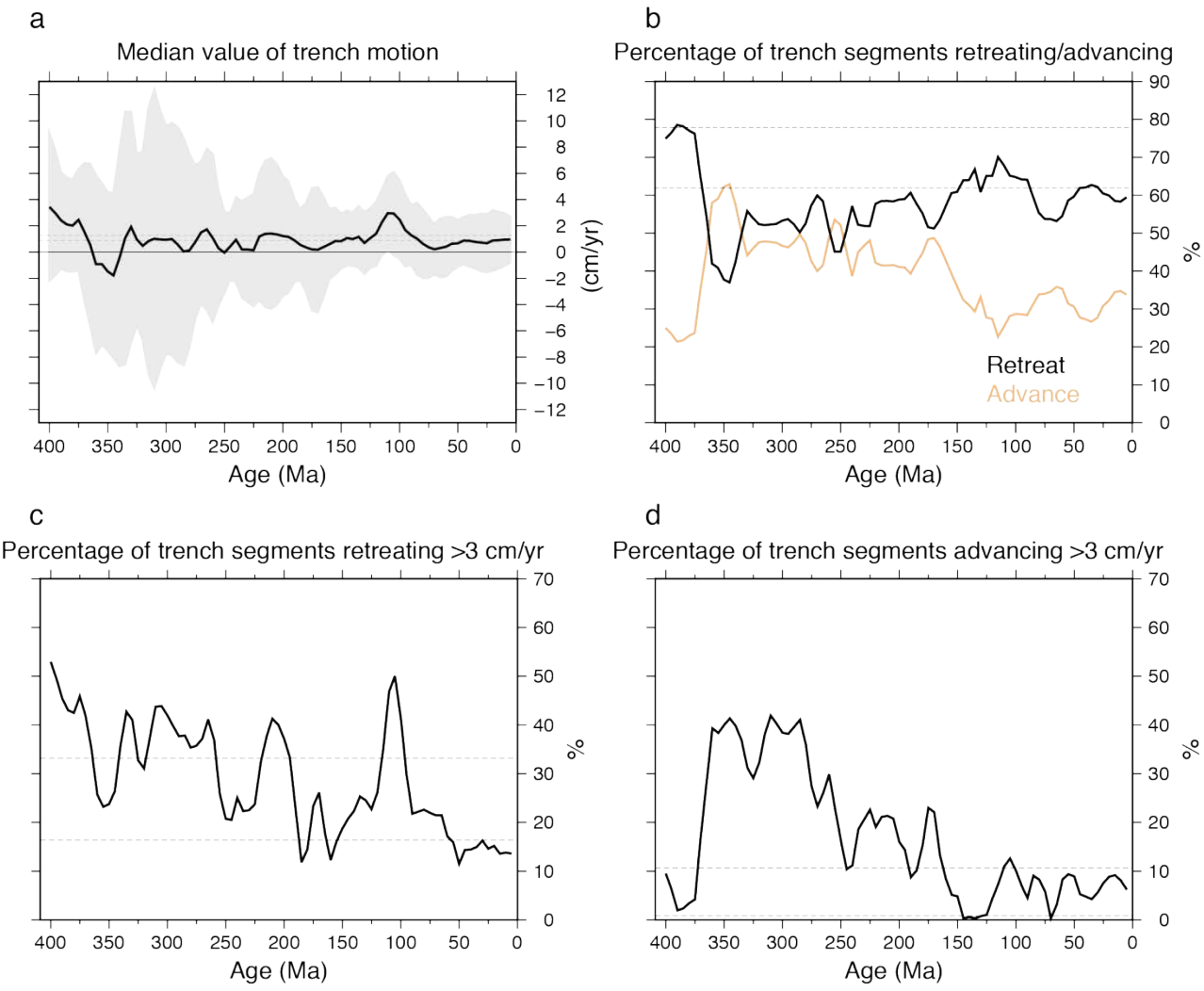


Figure 11

Trench migration statistics for the global model. In each graph the range of values computed by Schellart et al. (2008) for present-day are plotted as dashed lines. (a) Median value of trench motion, with the error envelope shaded grey. (b) Percentage of trench segments retreating (black line) and advancing (orange). The dashed lines correspond to the values calculated by Schellart et al. (2008) for retreat only. (c) Percentage of trenches retreating faster than 3 cm/yr. (d) Percentage of trenches advancing faster than 3 cm/yr. In each graph the values are extracted at 5 Myr intervals and then plotted as 10 Myr moving averages.

1063

1064 For most of the model timeframe the median value of trench motion remains close to, yet above 0
1065 cm/yr (indicating trench retreat) in agreement with the present-day findings of Schellart et al. (2008)
1066 (Figure 11a, dashed lines). There are, however, elevated values around 100 Ma, 350 Ma and 400 Ma,
1067 and between ~340–360 Ma the median falls below 0 cm/yr (indicating trench advance). Although the
1068 median values of the model are similar to those for present-day, the migration values are much more
1069 variable, as seen in the error envelope (Figure 11a), for times older than 150 Ma, particularly from
1070 380–260 Ma.

1071

1072 The model yields reasonable values for the percentage of retreating trench segments (Figure 11b). For
1073 most of the model trench retreat dominates over advance, except briefly at ~350 and ~250 Ma.
1074 Similarly to the findings of Williams et al. (2015) for the past 130 Myr, the percentage of segments
1075 retreating is generally slightly lower throughout the duration of the model than at present-day (Figure
1076 11b, dashed lines) (Schellart et al., 2008). According to our results the most similarity with present-
1077 day in terms of percentage of retreating and advancing segments is seen at the beginning of the model,
1078 >360 Ma.

1079

1080 In terms of the fastest retreating and advancing trenches (i.e. those moving faster than 3 cm/yr)
1081 (Figure 11c–d), a first-order observation is that the trench retreat speeds are fairly reasonable when
1082 compared with the range of values calculated by Schellart et al. (2008) for present-day (Figure 11c–d,
1083 dashed lines). The exceptions to this are seen in major spikes at ~400 Ma and 100 Ma, coinciding with
1084 almost 55% of trenches retreating faster than 3 cm/yr. In contrast, trench advance speeds are too high
1085 for most of the model, that is, from ~360–160 Ma the percentage of trench segments advancing faster
1086 than 3 cm/yr is up to four times that observed at present-day. As seen in Figure 12 the advancement of
1087 trenches in eastern and southeastern Panthalassa is particularly rapid between 350 and 250 Ma, for
1088 example the advancement of the Patagonian Plate subduction zone (comparison of red and orange
1089 lines) or the advancement of the western Gondwana subduction zone (comparison of orange and
1090 yellow lines). This is in contrast to the moderate retreat predicted over the past 200 Myr of the

western Gondwana/South American subduction zone (Figure 12, comparison of the green, blue and purple lines). During the Jurassic an example of rapid trench advance occurs at the eastern Asia subduction zone (Figure 12, comparison of green and light blue lines).

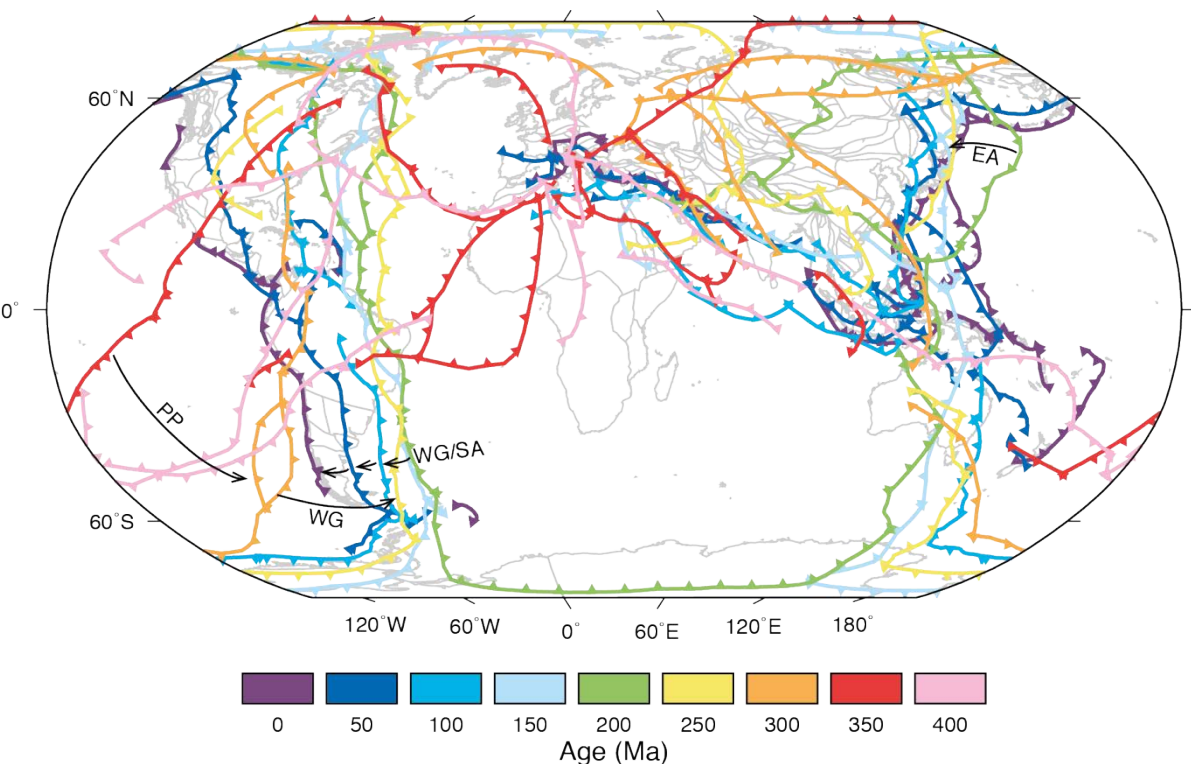


Figure 12

Modelled subduction zone locations at 50 Myr intervals, with present-day coastlines shown in grey. The distribution of subduction zones provides an indication of how mobile the trenches were over each interval. Examples of periods of high trench advance are identified, including advance of the Patagonian Plate (PP) trench from 350-300 Ma, the western Gondwana (WG) trench from 300-250 Ma and the eastern Asia (EA) trench from 200-150 Ma. In contrast, an example of trench retreat is that of the western Gondwana/South America (WG/SA) trench from 200 Ma to present-day.

Collins (2003) investigated trench locations through time from the late Paleozoic to present-day (see his Figure 2), based on a reconstruction from Scotese (2001). Our results (Figure 12) share some broad similarities in the predicted distribution of subduction zones, such as trench advance, although at lower magnitudes, in eastern and southeastern Panthalassa during the late Paleozoic and earliest Mesozoic (~425–195 Ma). Collins’ (2003) reconstruction incorporates fewer paleo-trenches coinciding with present-day Europe, the Pacific and northern Africa, and with narrower gaps between

1109 successive subduction zones trench migration also appears reduced during the late Paleozoic
1110 compared to our model.
1111
1112 In summary, trench behaviour trends over the past 410 Myr share many similarities with those
1113 computed at present-day (Schellart et al., 2008). In particular there is the expected dominance of
1114 trench retreat, and the percentage of trenches retreating faster than 3 cm/yr is reasonable throughout
1115 most of the model. A major divergence between trends in the model and what is expected based on
1116 present-day data, is a long period of very fast trench advance during much of the Paleozoic and
1117 Mesozoic (~360–160 Ma), dominated by trench behaviour in eastern and southeastern Panthalassa
1118 (Figure 12). A further apparent limitation of the model occurs at ~360 Ma where trench advance
1119 dominates over retreat and ~40% of advancing segments exceed 3 cm/yr compared with ~1–11% at
1120 present-day (Schellart et al., 2008). Interestingly in the period before 360 Ma the ratio of retreating to
1121 advancing trenches and the percentage of rapidly advancing trenches are very similar to present-day.
1122 However, the magnitude of trench retreat is likely too high during this time, with a high median value
1123 of trench motion and >50% of trenches retreating faster than 3 cm/yr.
1124
1125 These results are interesting for future studies to analyse absolute plate motions, and the global
1126 velocity trends described above in Section 5.3. For example, the period from 360–340 Ma, associated
1127 with rapid trench advance as well as the fastest global continental RMS speeds, coincides with the only
1128 prolonged period of significant counter-clockwise rotation of Africa (>20°).

1130 **6 Future directions**

1131
1132 It is essential that global models of plate motion undergo continuous regional refinements to both
1133 reflect the latest state of knowledge and test competing models. As new continental and marine
1134 geological and geophysical data become available, plate boundary evolution and plate motions may
1135 require modification, or even a complete overhaul.

1136

1137 Our analysis has highlighted specific regions and timeframes that may require refinement in future
1138 studies. In particular, we highlight the following as initial targets:

1139 (1) During the 260–160 Ma timeframe there is a noticeable decrease in the number of plates in the
1140 model and the ratio of small to large plates, reaching 9 and 1.3, respectively. We suggest that
1141 this timeframe be a target for future regional model refinement, in particular the addition of
1142 smaller plates. It is highly likely that there are plate boundaries missing in the model during
1143 this time, particularly as this coincides with Pangea fragmentation.

1144 (2) The global RMS speed of the continents exceeds 14 cm/yr at 360 Ma, more than quadruple that
1145 at present-day. We suggest future work may focus on testing the robustness of latest
1146 Devonian–Carboniferous absolute continental motions, such as by investigating alternative
1147 Paleozoic absolute reference frames, to confirm the current observed trends.

1148 (3) The rate of trench advance during most of the model from ~370–160 Ma is arguably too high.
1149 During this time the percentage of trenches advancing faster than 3 cm/yr reaches more than
1150 four times that computed for present-day (Schellart et al., 2008). We suggest that future work
1151 may investigate the cause of these high rates of motion and confirm if such high rates of trench
1152 advance are necessary to account for the model geological and geophysical constraints at these
1153 times. Again, this endeavour may also benefit from testing alternative absolute reference
1154 frames in both the Paleozoic and Mesozoic.

1155

1156 More broadly, we suggest that two pertinent and topical subjects for future studies, that were beyond
1157 the scope of our present study, are reinvestigating the Mesozoic–Cenozoic subduction history of
1158 Panthalassa and testing alternative models for the motion of Laurussia during the late Paleozoic prior
1159 to Pangea assembly.

1160

1161 Fast velocity anomalies imaged by seismic tomography in the mantle beneath the Pacific may
1162 represent sinking slabs from subduction zones not yet incorporated in the current plate
1163 reconstruction (van der Meer, 2012; Sigloch and Mihalynuk, 2013). While regional refinements in the

1164 northeastern Pacific, namely in western North America (Shephard et al., 2013) sought to better
1165 incorporate constraints from seismic tomography, a reinvestigation of subduction histories that
1166 considers tomographically-inferred slabs elsewhere in the Pacific remains to be undertaken. Such a
1167 study may result in the inclusion of additional plates in the model (van der Meer et al., 2012), the
1168 number of which is likely to be artificially low during the early–mid Mesozoic (Figure 6).

1169

1170 An interesting debate concerning the older part of the reconstruction focuses on the motion of
1171 Laurussia and its position relative to Gondwana prior to Pangea assembly. In one set of models
1172 (incorporated in this study) the Laurentian portion of Laurussia is located to the west of the South
1173 American portion of Gondwana during the Devonian–early Carboniferous (Figure 5a–b), such that the
1174 eastern Laurentian margin faces the western South American margin (present-day orientations)
1175 (Domeier and Torsvik, 2014; Torsvik et al., 2014). This model requires ~8500 km of relative, overall
1176 transform, motion between the two continents in order for Laurentia to reach its Pangea position
1177 during final supercontinent assembly. It also implies the existence of a wide Rheic Ocean between
1178 Baltica and present-day North Africa throughout the Devonian. In alternative reconstructions
1179 Laurentia remains close to the northwestern margin South America (present-day orientations), near
1180 its Pangea position throughout this timeframe (Scotese and McKerrow, 1990; McKerrow et al., 2000;
1181 Golonka, 2007). In these models the Rheic Ocean remains fairly narrow in the Devonian, in accordance
1182 with faunal affinities (Berdan, 1990; McKerrow et al., 2000; Boucot and Blodgett, 2001; Cocks and
1183 Torsvik, 2002), and Rheic Ocean closure proceeds through predominantly orthogonal, rather than
1184 transverse motion. We suggest that future work should test such an alternative reconstruction, to
1185 investigate whether such large shear zones are preserved in the geology and what the implications for
1186 the closure of the Rheic Ocean may be, as well as mantle evolution during Pangea assembly, resulting
1187 from an alternative subduction zone configuration and thus the location of slabs entering the mantle.

1188

1189 Finally, our work provides the framework for building more detailed regional reconstructions that
1190 span the Paleozoic to present-day, as well as extending the global reconstruction back further in time
1191 to the early Paleozoic (Torsvik et al., 2014) to capture the entire Phanerozoic in a single open-access

1192 topological model. This model does not yet capture the level of regional detail that has been proposed
1193 in many areas based on in-depth geological mapping, including the evolution of smaller and more
1194 detailed blocks, and marginal and back-arc basins such as along the Laurentian margins (van Staal et
1195 al., 2009; Nokleberg et al., 2000) and in the Tethyan realm (Stampfli et al., 2013). Stampfli et al. (2013)
1196 recently presented a regionally detailed global model with plate boundaries, however it is closed-
1197 source, which hinders its testability and adaptability.

1198 **7 Conclusions**

1199
1200 We present a continuous global plate reconstruction model that combines and builds upon the late
1201 Paleozoic, 410–250 Ma, model of Domeier and Torsvik (2014) and the Mesozoic-Cenozoic, 230–0 Ma,
1202 model of Müller et al. (2016). The model includes continuous and evolving plate boundaries with
1203 1 Myr temporal resolution. The constituent models were modified as little as possible to preserve their
1204 integrity and assist their future testing. Notable modifications that were required during the model
1205 harmonising process include altering the location and orientation of the late Paleozoic spreading ridge
1206 triple junction in Panthalassa, and adopting an updated absolute reference frame (Torsvik et al., 2012)
1207 for the period 230–100 Ma. A key regional contribution to this model is our reconstruction for the
1208 Baltica-derived Alexander Terrane that accreted to western North American in the Jurassic, and our
1209 model for opening and closure of the narrow Gravina Basin, also along western North America, in the
1210 Middle Jurassic–Early Cretaceous. Both models were built from a synthesis of regional geologic and
1211 kinematic studies.

1212
1213 We analysed the current global model for trends in the number of plates, plate size distribution, global
1214 plate and continental RMS speeds, and trench migration through time, comparing results with key
1215 present-day studies to elucidate global trends and test that the model is reasonable with respect to
1216 what we know about current plate behaviour. Although plate modelling constraints diminish back
1217 through time as a consequence of seafloor destruction and continental preservation, the current model
1218 performs well with respect to trends identified at present-day. For instance:

- (1) There are consistently fewer “large” plates ($\geq 10^{7.5}$ km²) than smaller ones. Except for during the period ~260–160 Ma, the ratio of smaller plates to large plates (~3.5–6.5) is similar to the present-day value (6.5), with the lower values observed during Pangea amalgamation which is as expected from a period of supercontinent growth.
- (2) The global RMS speeds of the continents are almost consistently less than those of the plates, which also include oceanic lithosphere.
- (3) The median value of trench motion remains close to, yet above 0 cm/yr for most of the model, reflecting dominance of trench retreat, similar to what is computed for present-day (Schellart et al., 2008). Additionally, the percentage of trenches retreating faster than 3 cm/yr is comparable to present-day.

It is essential that this model undergoes continual testing and refinement in order to improve on current potential shortcomings; incorporate additional regional complexity; and integrate new data, including alternative interpretations of existing, ambiguous data. In particular, we suggest that testing both absolute and relative aspects of plate motions in the Paleozoic and Mesozoic may help to mitigate extended periods of trench advance and global continental and plate RMS speeds that double to more than quadruple present-day values, whilst still being consistent with geological and geophysical data. Alternatively, driving mechanisms of these sustained periods of fast motions should be investigated.

This late Paleozoic to present-day model reconstructs the plates, including their boundaries, and therefore permits interdisciplinary studies that couple the mantle, surface and atmosphere to learn more about whole Earth evolution over deep time, including a supercontinent cycle. Finally, as the model is open-access it provides an important framework for producing a single continuous model that extends into the Precambrian that also has added regional complexity throughout, as well as the opportunity to test alternative regional reconstructions and absolute plate models.

1246 **Acknowledgements**

1247 K.J.M., K.T.M and R.D.M. were supported by Australian Research Council Discovery Grant
1248 DP130101946, S.Z. and S.E.W. were supported by ARC grant IH130200012, S.E.W. was also supported
1249 by SIEF project RP 04-174, M.S. was supported by Australian Research Council Future Fellowship
1250 FT130101564. We thank John Cannon and Michael Tetley for GPlates technical support. We are
1251 grateful to Mathew Domeier and Alan Collins for providing thoughtful and constructive reviews that
1252 improved the manuscript. Figures 2-12 were made using the Generic Mapping Tools (GMT) software
1253 (Wessel et al., 2013). The digital plate model, including rotation and geometry files, are available as
1254 supplementary material and can also be downloaded from the EarthByte Group’s website
1255 (www.earthbyte.org).

1256

1257 **References**

1258 Amato, J.M., Rioux, M.E., Kelemen, P.B., Gehrels, G.E., Clift, P.D., Pavlis, T.L., Draut, A.E., 2007. U-Pb
1259 geochronology of volcanic rocks from the Jurassic Talkeetna Formation and detrital zircons from
1260 prearc and postarc sequences: Implications for the age of magmatism and inheritance in the
1261 Talkeetna arc. Geological Society of America Special Papers 431, 253-271.

1262 Barnett-Moore, N., Müller, R.D., Williams, S., Skogseid, J., Seton, M., in press. A reconstruction of the
1263 North Atlantic since the earliest Jurassic. Basin Research.

1264 Barth, A.P., Tosdal, R.M., Wooden, J.L., Howard, K.A., 1997. Triassic plutonism in southern California:
1265 Southward younging of arc initiation along a truncated continental margin. Tectonics 16, 290-304.

1266 Bazard, D.R., Butler, R.F., Gehrels, G., Soja, C.M., 1995. Early Devonian paleomagnetic data from the
1267 Lower Devonian Karheen Formation suggest Laurentia-Baltica connection for the Alexander
1268 terrane. Geology 23, 707-710.

1269 Beranek, L.P., Mortensen, J.K., 2011. The timing and provenance record of the Late Permian Klondike
1270 orogeny in northwestern Canada and arc-continent collision along western North America.
1271 Tectonics 30.

1272 Beranek, L.P., van Staal, C.R., McClelland, W.C., Israel, S., Mihalynuk, M.G., 2013. Baltican crustal
1273 provenance for Cambrian–Ordovician sandstones of the Alexander terrane, North American
1274 Cordillera: evidence from detrital zircon U–Pb geochronology and Hf isotope geochemistry. *Journal*
1275 *of the Geological Society* 170, 7-18.

1276 Beranek, L.P., van Staal, C.R., McClelland, W.C., Israel, S., Mihalynuk, M.G., 2013. Detrital zircon Hf
1277 isotopic compositions indicate a northern Caledonian connection for the Alexander terrane.
1278 *Lithosphere* 5, 163-168.

1279 Berdan, J.M., 1990. The Silurian and Early Devonian biogeography of ostracodes in North America.
1280 *Geological Society, London, Memoirs* 12, 223-231.

1281 Berg, H.C., Jones, D.L., Richter, D.H., 1972. Gravina-Nutzotin Belt; tectonic significance of an upper
1282 Mesozoic sedimentary and volcanic sequence in southern and southeastern Alaska, U.S. Geological
1283 Survey, Geological survey research, pp. D1-D24.

1284 Berner, R.A., Lasaga, A.C., Garrels, R.M., 1983. The carbonate-silicate geochemical cycle and its effect on
1285 atmospheric carbon dioxide over the past 100 million years. *American Journal of Science* 283, 641-
1286 683.

1287 Bird, P., 2003. An updated digital model of plate boundaries. *Geochemistry, Geophysics, Geosystems* 4.

1288 Blodgett, R.B., Boucot, A.J., Rohr, D.M., Pedder, A.E.H., 2010. The Alexander Terrane of Alaska-a
1289 Displaced Fragment of Northeast Russia?: Evidence from Silurian-middle Devonian Megafossils and
1290 Stratigraphy. *Memoirs of the Association of Australasian Palaeontologists* 39, 323-339.

1291 Boucot, A.J., Blodgett, R.B., 2001. Silurian-Devonian biogeography, in: Brunton, C.H.C., Cocks, L.R.M.,
1292 Long, S. (Eds.), *Brachiopods past and present Systematics Association Special Volume Series*,
1293 London.

1294 Bower, D.J., Gurnis, M., Seton, M., 2013. Lower mantle structure from paleogeographically constrained
1295 dynamic Earth models. *Geochemistry, Geophysics, Geosystems* 14, 44-63.

1296 Boyden, J.A., Müller, R.D., Gurnis, M., Torsvik, T.H., Clark, J.A., Turner, M., Ivey-Law, H., Watson, R.J.,
1297 Cannon, J.S., 2011. Next-generation plate-tectonic reconstructions using GPlates, in: G.R., K., Baru, C.
1298 (Eds.), *Geoinformatics: Cyberinfrastructure for the Solid Earth Sciences*. Cambridge University
1299 Press, Cambridge, pp. 95-114.

1300 Brown, D., Spadea, P., Puchkov, V., Alvarez-Marron, J., Herrington, R., Willner, A.P., Hetzel, R.,
 1301 Gorozhanina, Y., Juhlin, C., 2006. Arc-continent collision in the Southern Urals. *Earth-Science*
 1302 *Reviews* 79, 261-287.

1303 Bull, A.L., Domeier, M., Torsvik, T.H., 2014. The effect of plate motion history on the longevity of deep
 1304 mantle heterogeneities. *Earth and Planetary Science Letters* 401, 172-182.

1305 Burke, K., Torsvik, T.H., 2004. Derivation of large igneous provinces of the past 200 million years from
 1306 long-term heterogeneities in the deep mantle. *Earth and Planetary Science Letters* 227, 531-538.

1307 Butler, R.F., Gehrels, G.E., Bazard, D.R., 1997. Paleomagnetism of Paleozoic strata of the Alexander
 1308 terrane, southeastern Alaska. *Geological Society of America Bulletin* 109, 1372-1388.

1309 Butterworth, N.P., Talsma, A.S., Müller, R.D., Seton, M., Bunge, H.-P., Schuberth, B.S.A., Shephard, G.E.,
 1310 Heine, C., 2014. Geological, tomographic, kinematic and geodynamic constraints on the dynamics of
 1311 sinking slabs. *Journal of Geodynamics* 73, 1-13.

1312 Cocks, L.R.M., Torsvik, T.H., 2002. Earth geography from 500 to 400 million years ago: a faunal and
 1313 palaeomagnetic review. *Journal of the Geological Society* 159, 631-644.

1314 Collins, W.J., 2003. Slab pull, mantle convection, and Pangaeon assembly and dispersal. *Earth and*
 1315 *Planetary Science Letters* 205, 225-237.

1316 Colpron, M., Crowley, J.L., Gehrels, G., Long, D.G.F., Murphy, D.C., Beranek, L., Bickerton, L., 2015. Birth
 1317 of the northern Cordilleran orogen, as recorded by detrital zircons in Jurassic synorogenic strata
 1318 and regional exhumation in Yukon. *Lithosphere* 7, 541-562.

1319 Colpron, M., Nelson, J.L., 2009. A Palaeozoic Northwest Passage: Incursion of Caledonian, Baltican and
 1320 Siberian terranes into eastern Panthalassa, and the early evolution of the North American
 1321 Cordillera. *Geological Society, London, Special Publications* 318, 273-307.

1322 Colpron, M., Nelson, J.L., 2011. Chapter 31 A Palaeozoic NW Passage and the Timanian, Caledonian and
 1323 Uralian connections of some exotic terranes in the North American Cordillera. *Geological Society,*
 1324 *London, Memoirs* 35, 463-484.

1325 Condie, K., Pisarevsky, S.A., Korenaga, J., Gardoll, S., 2015. Is the rate of supercontinent assembly
 1326 changing with time? *Precambrian Research* 259, 278-289.

1327 Crawford, M.L., Hollister, L.S., Woodsworth, G.J., 1987. Crustal deformation and regional
1328 metamorphism across a terrane boundary, Coast Plutonic Complex, British Columbia. *Tectonics* 6,
1329 343-361.

1330 Dickinson, W.R., 2004. Evolution of the North American cordillera. *Annu. Rev. Earth Planet. Sci.* 32, 13-
1331 45.

1332 Dickinson, W.R., 2006. Geotectonic evolution of the Great Basin. *Geosphere* 2, 353-368.

1333 Domeier, M., in press. A plate tectonic scenario for the Iapetus and Rheic oceans. *Gondwana Research*.

1334 Domeier, M., Torsvik, T.H., 2014. Plate tectonics in the late Paleozoic. *Geoscience Frontiers* 5, 303-350.

1335 Flament, N., Gurnis, M., Müller, R.D., Bower, D.J., Husson, L., 2015. Influence of subduction history on
1336 South American topography. *Earth and Planetary Science Letters* 430, 9-18.

1337 Flowers, R.M., Ault, A.K., Kelley, S.A., Zhang, N., Zhong, S., 2012. Epeirogeny or eustasy? Paleozoic–
1338 Mesozoic vertical motion of the North American continental interior from thermochronometry and
1339 implications for mantle dynamics. *Earth and Planetary Science Letters* 317, 436-445.

1340 Forsyth, D., Uyeda, S., 1975. On the relative importance of the driving forces of plate motion.
1341 *Geophysical Journal International* 43, 163-200.

1342 Gardner, M.C., Bergman, S.C., Cushing, G.W., MacKevett, E.M., Plafker, G., Campbell, R.B., Dodds, C.J.,
1343 McClelland, W.C., Mueller, P.A., 1988. Pennsylvanian pluton stitching of Wrangellia and the
1344 Alexander terrane, Wrangell Mountains, Alaska. *Geology* 16, 967-971.

1345 Gehrels, G.E., 2001. Geology of the Chatham Sound region, southeast Alaska and coastal British
1346 Columbia. *Canadian Journal of Earth Sciences* 38, 1579-1599.

1347 Gehrels, G.E., Butler, R.F., Bazard, D.R., 1996. Detrital zircon geochronology of the Alexander terrane,
1348 southeastern Alaska. *Geological Society of America Bulletin* 108, 722-734.

1349 Gehrels, G.E., McClelland, W.C., Samson, S.D., Patchett, P.J., Orchard, M.J., 1992. Geology of the western
1350 flank of the Coast Mountains between Cape Fanshaw and Taku Inlet, southeastern Alaska. *Tectonics*
1351 11, 567-585.

1352 Gehrels, G.E., Rusmore, M., Woodsworth, G., Crawford, M., Andronicos, C., Hollister, L., Patchett, J.,
1353 Ducea, M., Butler, R., Klepeis, K., 2009. U-Th-Pb geochronology of the Coast Mountains batholith in

1354 north-coastal British Columbia: Constraints on age and tectonic evolution. Geological Society of
1355 America Bulletin 121, 1341-1361.

1356 Gehrels, G.E., Saleeby, J.B., 1987. Geologic framework, tectonic evolution, and displacement history of
1357 the Alexander terrane. Tectonics 6, 151-173.

1358 Gehrels, G.E., Saleeby, J.B., Berg, H.C., 1983. Preliminary description of the Late Silurian-Early Devonian
1359 Klakas Orogeny in the southern Alexander terrane, southeastern Alaska, Pre-Jurassic rocks in
1360 western North American suspect terranes. Society of Economic Paleontologists and Mineralogists,
1361 pp. 131-141.

1362 Gernon, T.M., Hincks, T.K., Tyrrell, T., Rohling, E.J., Palmer, M.R., 2016. Snowball Earth ocean chemistry
1363 driven by extensive ridge volcanism during Rodinia breakup. Nature Geosci 9, 242-248.

1364 Gibbons, A.D., Zahirovic, S., Müller, R.D., Whittaker, J.M., Yatheesh, V., 2015. A tectonic model
1365 reconciling evidence for the collisions between India, Eurasia and intra-oceanic arcs of the central-
1366 eastern Tethys. Gondwana Research.

1367 Golonka, J., 2007. Phanerozoic paleoenvironment and paleolithofacies maps: late Paleozoic.
1368 Geologia/Akademia Górniczo-Hutnicza im. Stanisława Staszica w Krakowie 33, 145-209.

1369 Gordon, R.G., Jurdy, D.M., 1986. Cenozoic global plate motions. Journal of Geophysical Research: Solid
1370 Earth (1978–2012) 91, 12389-12406.

1371 Grove, M., Gehrels, G.E., Cotkin, S.J., Wright, J.E., Zou, H., 2008. Non-Laurentian cratonic provenance of
1372 Late Ordovician eastern Klamath blueschists and a link to the Alexander terrane. Geological Society
1373 of America Special Papers 438, 223-250.

1374 Gurnis, M., Torsvik, T.H., 1994. Rapid drift of large continents during the late Precambrian and
1375 Paleozoic: Paleomagnetic constraints and dynamic models. Geology 22, 1023-1026.

1376 Gurnis, M., Turner, M., Zahirovic, S., DiCaprio, L., Spasojevic, S., Müller, R., Boyden, J., Seton, M., Manea,
1377 V.C., Bower, D.J., 2012. Plate Tectonic Reconstructions with Continuously Closing Plates. Computers
1378 & Geosciences 38, 35-42.

1379 Hassan, R., Flament, N., Gurnis, M., Bower, D.J., Müller, D., 2015. Provenance of plumes in global
1380 convection models. Geochemistry, Geophysics, Geosystems 16, 1465-1489.

1381 Hassan, R., Müller, R.D., Gurnis, M., Williams, S.E., Flament, N., 2016. A rapid burst in hotspot motion
1382 through the interaction of tectonics and deep mantle flow. *Nature* 533, 239-242.

1383 Hosseinpour, M., Williams, S., Seton, M., Barnett-Moore, N., Müller, R.D., 2016. Tectonic evolution of
1384 Western Tethys from Jurassic to present day: coupling geological and geophysical data with seismic
1385 tomography models. *International Geology Review*, 1-30.

1386 Jagoutz, O., Royden, L., Holt, A.F., Becker, T.W., 2015. Anomalously fast convergence of India and
1387 Eurasia caused by double subduction. *Nature Geoscience* 8, 475-478.

1388 Johnson, K., Schwartz, J.J., Žák, J., Verner, K., Barnes, C.G., Walton, C., Wooden, J.L., Wright, J.E., Kistler,
1389 R.W., 2015. Composite Sunrise Butte pluton: Insights into Jurassic–Cretaceous collisional tectonics
1390 and magmatism in the Blue Mountains Province, northeastern Oregon. *Geological Society of*
1391 *America Special Papers* 513, 377-398.

1392 Kapp, P.A., Gehrels, G.E., 1998. Detrital zircon constraints on the tectonic evolution of the Gravina belt,
1393 southeastern Alaska. *Canadian Journal of Earth Sciences* 35, 253-268.

1394 Lee, C.-T.A., Shen, B., Slotnick, B.S., Liao, K., Dickens, G.R., Yokoyama, Y., Lenardic, A., Dasgupta, R.,
1395 Jellinek, M., Lackey, J.S., 2013. Continental arc–island arc fluctuations, growth of crustal carbonates,
1396 and long-term climate change. *Geosphere* 9, 21-36.

1397 Lithgow-Bertelloni, C., Richards, M.A., 1998. The dynamics of Cenozoic and Mesozoic plate motions.
1398 *Reviews of Geophysics* 36, 27-78.

1399 Liu, J., Tran, M.-D., Tang, Y., Nguyen, Q.-L., Tran, T.-H., Wu, W., Chen, J., Zhang, Z., Zhao, Z., 2012. Permo-
1400 Triassic granitoids in the northern part of the Truong Son belt, NW Vietnam: geochronology,
1401 geochemistry and tectonic implications. *Gondwana Research* 22, 628-644.

1402 Mallard, C., Coltice, N., Seton, M., Müller, R.D., Tackley, P.J., 2016. Subduction controls the distribution
1403 and fragmentation of Earth's tectonic plates. *Nature advance online publication*.

1404 Matthews, K.J., Seton, M., Müller, R.D., 2012. A global-scale plate reorganization event at 105– 100Ma.
1405 *Earth and Planetary Science Letters* 355, 283-298.

1406 McClelland, W.C., Gehrels, G.E., 1990. Geology of the Duncan Canal shear zone: Evidence for Early to
1407 Middle Jurassic deformation of the Alexander terrane, southeastern Alaska. *Geological Society of*
1408 *America Bulletin* 102, 1378-1392.

1409 McClelland, W.C., Gehrels, G.E., Saleeby, J.B., 1992. Upper Jurassic-lower Cretaceous basinal strata
 1410 along the Cordilleran margin: Implications for the accretionary history of the
 1411 Alexander-Wrangellia-Peninsular terrane. *Tectonics* 11, 823-835.

1412 McKerrow, W.S., MacNiocaill, C., Ahlberg, P.E., Clayton, G., Cleal, C.J., Eagar, R.M.C., 2000. The late
 1413 Palaeozoic relations between Gondwana and Laurussia. Geological Society, London, Special
 1414 Publications 179, 9-20.

1415 McNamara, A.K., Zhong, S., 2005. Thermochemical structures beneath Africa and the Pacific Ocean.
 1416 *Nature* 437, 1136-1139.

1417 Meert, J.G., van der Voo, R., Powell, C.M., Li, Z.-X., McElhinny, M.W., Chen, Z., Symons, D.T.A., 1993. A
 1418 plate-tectonic speed limit? *Nature* 363, 216-217.

1419 Mihalynuk, M.G., Erdmer, P., Ghent, E.D., Cordey, F., Archibald, D.A., Friedman, R.M., Johannson, G.G.,
 1420 2004. Coherent French Range blueschist: Subduction to exhumation in < 2.5 my? Geological Society
 1421 of America Bulletin 116, 910-922.

1422 Mihalynuk, M.G., Nelson, J., Diakow, L.J., 1994. Cache Creek terrane entrapment: oroclinal paradox
 1423 within the Canadian Cordillera. *Tectonics* 13, 575-595.

1424 Miller, E.L., Kuznetsov, N., Soboleva, A., Udoratina, O., Grove, M.J., Gehrels, G., 2011. Baltica in the
 1425 Cordillera? *Geology* 39, 791-794.

1426 Monger, J.W.H., van Der Heyden, P., Journeay, J.M., Evenchick, C.A., Mahoney, J.B., 1994. Jurassic-
 1427 Cretaceous basins along the Canadian Coast Belt: Their bearing on pre-mid-Cretaceous sinistral
 1428 displacements. *Geology* 22, 175-178.

1429 Moore, T.E., Wallace, W.K., Bird, K.J., Karl, S.M., Mull, C.G., Dillon, J.T., 1994. Geology of northern Alaska,
 1430 in: Plafker, G., Berg, H.C. (Eds.), *The Geology of Alaska*. Geological Society of America, pp. 49-138.

1431 Morra, G., Seton, M., Quevedo, L., Müller, R.D., 2013. Organization of the tectonic plates in the last 200
 1432 Myr. *Earth and Planetary Science Letters* 373, 93-101.

1433 Mortensen, J.K., 1992. Pre-mid-Mesozoic tectonic evolution of the Yukon-Tanana terrane, Yukon and
 1434 Alaska. *Tectonics* 11, 836-853.

1435 Müller, R.D., Seton, M., Zahirovic, S., Williams, S.E., Matthews, K.J., Wright, N.M., Shephard, G.E.,
 1436 Maloney, K., Barnett-Moore, N., Hosseinpour, M., 2016. Ocean Basin Evolution and Global-Scale

1437 Plate Reorganization Events Since Pangea Breakup. *Annual Review of Earth and Planetary Sciences*
1438 44.

1439 Nelson, J., Friedman, R., 2004. Superimposed Quesnel (late Paleozoic Jurassic) and Yukon Tanana
1440 (Devonian Mississippian) arc assemblages, Cassiar Mountains, northern British Columbia: field, U
1441 Pb, and igneous petrochemical evidence. *Canadian Journal of Earth Sciences* 41, 1201-1235.

1442 Nelson, J.L., Colpron, M., Piercey, S.J., Dusel-Bacon, C., Murphy, D.C., Roots, C.F., 2006. Paleozoic tectonic
1443 and metallogenetic evolution of pericratonic terranes in Yukon, northern British Columbia and
1444 eastern Alaska, in: Colpron, M., Nelson, J.L. (Eds.), *Paleozoic evolution and metallogeny of*
1445 *pericratonic terranes at the ancient Pacific margin of North America, Canadian and Alaskan*
1446 *Cordillera*. Geological Association of Canada Special Paper, pp. 323-360.

1447 Nokleberg, W.J., Parfenov, L.M., Monger, J.W.H., Norton, I.O., Khanchuk, A.I., Stone, D.B., Scotese, C.R.,
1448 Scholl, D.W., Fujita, K., 2000. Phanerozoic tectonic evolution of the Circum-North Pacific.
1449 Professional Paper 1626, US Department of the Interior, US Geological Survey.

1450 Piercey, S.J., Nelson, J.L., Colpron, M., Dusel-Bacon, C., Simard, R.-L., Roots, C.F., 2006. Paleozoic
1451 magmatism and crustal recycling along the ancient Pacific margin of North America, northern
1452 Cordillera, in: Colpron, M., Nelson, J.L. (Eds.), *Paleozoic evolution and metallogeny of pericratonic*
1453 *terranes at the ancient Pacific margin of North America, Canadian and Alaskan Cordillera*.
1454 Geological Association of Canada Special Paper, pp. 281-322.

1455 Saleeby, J.B., 2000. Geochronologic investigations along the Alexander-Taku terrane boundary,
1456 southern Revillagigedo Island to Cape Fox areas, southeast Alaska, in: Stowell, H.H., McClelland,
1457 W.C. (Eds.), *Tectonics of the Coast Mountains, Southeastern Alaska and British Columbia*. Geological
1458 Society of America Special Paper 343, Boulder, Colorado.

1459 Saleeby, J.B., 2011. Geochemical mapping of the Kings-Kaweah ophiolite belt, California—Evidence for
1460 progressive mélangé formation in a large offset transform-subduction initiation environment.
1461 Geological Society of America Special Papers 480, 31-73.

1462 Saleeby, J.B., Dunne, G., 2015. Temporal and tectonic relations of early Mesozoic arc magmatism,
1463 southern Sierra Nevada, California. Geological Society of America Special Papers 513, SPE513-505.

1464 Schellart, W.P., Stegman, D.R., Freeman, J., 2008. Global trench migration velocities and slab migration
 1465 induced upper mantle volume fluxes: Constraints to find an Earth reference frame based on
 1466 minimizing viscous dissipation. *Earth-Science Reviews* 88, 118-144.

1467 Schettino, A., Turco, E., 2011. Tectonic history of the western Tethys since the Late Triassic. *Geological*
 1468 *Society of America Bulletin* 123, 89-105.

1469 Schwartz, J.J., Snoke, A.W., Cordey, F., Johnson, K., Frost, C.D., Barnes, C.G., LaMaskin, T.A., Wooden, J.L.,
 1470 2011. Late Jurassic magmatism, metamorphism, and deformation in the Blue Mountains Province,
 1471 northeast Oregon. *Geological Society of America Bulletin*, B30327. 30321.

1472 Scotese, C.R., 2001. Atlas of Earth History 2001: Paleomap Progress Report 90-0497, Department of
 1473 Geology, University of Texas, Arlington, TX.

1474 Scotese, C.R., McKerrow, W.S., 1990. Revised world maps and introduction. *Geological Society, London,*
 1475 *Memoirs* 12, 1-21.

1476 Seton, M., Müller, R.D., Zahirovic, S., Gaina, C., Torsvik, T., Shephard, G.E., Talsma, A., Gurnis, M., Turner,
 1477 M., Maus, S., 2012. Global continental and ocean basin reconstructions since 200 Ma. *Earth-Science*
 1478 *Reviews* 113, 212-270.

1479 Shephard, G.E., Bunge, H.-P., Schuberth, B.S.A., Müller, R.D., Talsma, A.S., Moder, C., Landgrebe, T.C.W.,
 1480 2012. Testing absolute plate reference frames and the implications for the generation of
 1481 geodynamic mantle heterogeneity structure. *Earth and Planetary Science Letters* 317, 204-217.

1482 Shephard, G.E., Flament, N., Williams, S., Seton, M., Gurnis, M., Müller, R.D., 2014. Circum-Arctic mantle
 1483 structure and long-wavelength topography since the Jurassic. *Journal of Geophysical Research:*
 1484 *Solid Earth* 119, 7889-7908.

1485 Shephard, G.E., Müller, R.D., Seton, M., 2013. The tectonic evolution of the Arctic since Pangea breakup:
 1486 Integrating constraints from surface geology and geophysics with mantle structure. *Earth-Science*
 1487 *Reviews* 124, 148-183.

1488 Sigloch, K., Mihalynuk, M.G., 2013. Intra-oceanic subduction shaped the assembly of Cordilleran North
 1489 America. *Nature* 496, 50-56.

1490 Soja, C.M., Antoshkina, A.I., 1997. Coeval development of Silurian stromatolite reefs in Alaska and the
 1491 Ural Mountains: Implications for paleogeography of the Alexander terrane. *Geology* 25, 539-542.

1492 Stampfli, G.M., Borel, G.D., 2002. A plate tectonic model for the Paleozoic and Mesozoic constrained by
 1493 dynamic plate boundaries and restored synthetic oceanic isochrons. *Earth & Planetary Science*
 1494 *Letters* 196, 17-33.

1495 Stampfli, G.M., Hochard, C., V  rard, C., Wilhem, C., vonRaumer, J., 2013. The formation of Pangea.
 1496 *Tectonophysics* 593, 1-19.

1497 Steinberger, B., Torsvik, T.H., 2008. Absolute plate motions and true polar wander in the absence of
 1498 hotspot tracks. *Nature* 452, 620-623.

1499 Tochilin, C.J., Gehrels, G.E., Nelson, J., Mahoney, J.B., 2014. U-Pb and Hf isotope analysis of detrital
 1500 zircons from the Banks Island assemblage (coastal British Columbia) and southern Alexander
 1501 terrane (southeast Alaska). *Lithosphere* 6, 200-215.

1502 Torsvik, T.H., Cocks, L.R.M., 2004. Earth geography from 400 to 250 Ma: a palaeomagnetic, faunal and
 1503 facies review. *Journal of the Geological Society* 161, 555-572.

1504 Torsvik, T.H., M  ller, R.D., van der Voo, R., Steinberger, B., Gaina, C., 2008. Global plate motion frames:
 1505 toward a unified model. *Reviews of Geophysics* 46.

1506 Torsvik, T.H., Steinberger, B., Cocks, L.R.M., Burke, K., 2008. Longitude: Linking Earth's ancient surface
 1507 to its deep interior. *Earth and Planetary Science Letters* 276, 273-282.

1508 Torsvik, T.H., van der Voo, R., Doubrovine, P.V., Burke, K., Steinberger, B., Ashwal, L.D., Tr  nnes, R.G.,
 1509 Webb, S.J., Bull, A.L., 2014. Deep mantle structure as a reference frame for movements in and on the
 1510 Earth. *Proceedings of the National Academy of Sciences* 111, 8735-8740.

1511 Torsvik, T.H., van der Voo, R., Preeden, U., Mac Niocaill, C., Steinberger, B., Doubrovine, P.V., van
 1512 Hinsbergen, D.J.J., Domeier, M., Gaina, C., Tohver, E., Meert, J.G., McCausland, P.J.A., Cocks, L.R.M.,
 1513 2012. Phanerozoic polar wander, palaeogeography and dynamics. *Earth-Science Reviews* 114, 325-
 1514 368.

1515 Trop, J.M., Ridgway, K.D., 2007. Mesozoic and Cenozoic tectonic growth of southern Alaska: A
 1516 sedimentary basin perspective. *Geological Society of America Special Papers* 431, 55-94.

1517 Trop, J.M., Ridgway, K.D., Manuszak, J.D., Layer, P., 2002. Mesozoic sedimentary-basin development on
 1518 the allochthonous Wrangellia composite terrane, Wrangell Mountains basin, Alaska: A long-term

1519 record of terrane migration and arc construction. *Geological Society of America Bulletin* 114, 693-
1520 717.

1521 van der Heyden, P., 1992. A Middle Jurassic to Early Tertiary Andean-Sierran Arc Model for the Coast
1522 Belt of British Columbia. *Tectonics* 11, 82-97.

1523 van der Meer, D.G., Spakman, W., van Hinsbergen, D.J.J., Amaru, M.L., Torsvik, T.H., 2010. Towards
1524 absolute plate motions constrained by lower-mantle slab remnants. *Nature Geoscience* 3, 36-40.

1525 van der Meer, D.G., Torsvik, T.H., Spakman, W., van Hinsbergen, D.J.J., Amaru, M.L., 2012. Intra-
1526 Panthalassa Ocean subduction zones revealed by fossil arcs and mantle structure. *Nature*
1527 *Geoscience* 5, 215-219.

1528 van der Meer, D.G., Zeebe, R.E., van Hinsbergen, D.J.J., Sluijs, A., Spakman, W., Torsvik, T.H., 2014. Plate
1529 tectonic controls on atmospheric CO₂ levels since the Triassic. *Proceedings of the National*
1530 *Academy of Sciences* 111, 4380-4385.

1531 van Hinsbergen, D.J.J., Steinberger, B., Doubrovine, P.V., Gassmüller, R., 2011. Acceleration and
1532 deceleration of India-Asia convergence since the Cretaceous: Roles of mantle plumes and
1533 continental collision. *Journal of Geophysical Research: Solid Earth* (1978–2012) 116.

1534 van Staal, C.R., Whalen, J.B., Valverde-Vaquero, P., Zagorevski, A., Rogers, N., 2009. Pre-Carboniferous,
1535 episodic accretion-related, orogenesis along the Laurentian margin of the northern Appalachians.
1536 *Geological Society, London, Special Publications* 327, 271-316.

1537 Veevers, J.J., 2000. Change of tectono-stratigraphic regime in the Australian plate during the 99 Ma
1538 (mid-Cretaceous) and 43 Ma (mid-Eocene) swerves of the Pacific. *Geology* 28, 47-50.

1539 Wessel, P., Kroenke, L.W., 2008. Pacific absolute plate motion since 145 Ma: An assessment of the fixed
1540 hot spot hypothesis. *Journal of Geophysical Research* 113, B06101.

1541 Wessel, P., Smith, W.H.F., Scharroo, R., Luis, J., Wobbe, F., 2013. *Generic Mapping Tools: Improved*
1542 *Version Released*. *Eos, Transactions American Geophysical Union* 94, 409-410.

1543 Whittaker, J.M., Müller, R.D., Leitchnikov, G., Stagg, H., Sdrolias, M., Gaina, C., Goncharov, A., 2007.
1544 Major Australian-Antarctic plate reorganization at Hawaiian-Emperor bend time. *Science* 318, 83-
1545 86.

Williams, S., Flament, N., Müller, R.D., Butterworth, N., 2015. Absolute plate motions since 130 Ma constrained by subduction zone kinematics. *Earth and Planetary Science Letters* 418, 66-77.

Wright, J.E., Wyld, S.J., 2006. Gondwanan, Iapetan, Cordilleran interactions: A geodynamic model for the Paleozoic tectonic evolution of the North American Cordillera. *Paleogeography of the North American cordillera: Evidence for and against large-scale displacements: Geological Association of Canada Special Paper* 46, 377-408.

Wu, Y.-B., Zheng, Y.-F., 2013. Tectonic evolution of a composite collision orogen: an overview on the Qinling–Tongbai–Hong'an–Dabie–Sulu orogenic belt in central China. *Gondwana Research* 23, 1402-1428.

Wyld, S.J., 1991. Permo-Triassic tectonism in volcanic arc sequences of the western US Cordillera and implications for the Sonoma orogeny. *Tectonics* 10, 1007-1017.

Zahirovic, S., Müller, R.D., Seton, M., Flament, N., 2015. Tectonic speed limits from plate kinematic reconstructions. *Earth and Planetary Science Letters* 418, 40-52.

Zahirovic, S., Seton, M., Müller, R.D., 2014. The Cretaceous and Cenozoic tectonic evolution of Southeast Asia. *Solid Earth* 5, 227-273.

Zhang, N., Zhong, S., Flowers, R.M., 2012. Predicting and testing continental vertical motion histories since the Paleozoic. *Earth and Planetary Science Letters* 317–318, 426-435.

Zhong, S., Liu, X., 2016. The long-wavelength mantle structure and dynamics and implications for large-scale tectonics and volcanism in the Phanerozoic. *Gondwana Research* 29, 83-104.

Zhong, S., Rudolph, M.L., 2015. On the temporal evolution of long-wavelength mantle structure of the Earth since the early Paleozoic. *Geochemistry, Geophysics, Geosystems* 16, 1599-1615.

Zhu, D.-C., Zhao, Z.-D., Niu, Y., Dilek, Y., Mo, X.-X., 2011. Lhasa terrane in southern Tibet came from Australia. *Geology* 39, 727-730.

Highlights:

- A continuous global plate reconstruction model is presented that spans 410–0 Ma
- The model is digital and open-access
- A new regional model for the Baltica-derived Alexander Terrane is incorporated
- Plate sizes, plate and continent speeds and trench migration patterns are analysed

File(s) excluded from PDF

The following file(s) will not be converted:

supplementary_readme_file_PlateModel_Matthews++.txt

AnimationS1_Matthews++.mov

AnimationS2_Matthews++.mov

AnimationS3_Matthews++.mov

Please click 'Download zip file' to download the most recent files related to this submission.